AMERICAN SOCIETY FOR MICROBIOLOGY | mBio

Check for updates

| Parasitology | Research Article

CDPK2A and CDPK1 form a signaling module upstream of *Toxoplasma* motility

Emily Shortt,[1] Caroline G. Hackett,[1] Rachel V. Stadler,[2] Robyn S. Kent,[2] Alice L. Herneisen,[1,3] Gary E. Ward,[2] Sebastian Lourido[1,3]

AUTHOR AFFILIATIONS See affiliation list on p. 21.

ABSTRACT In apicomplexan parasites, the transition between replication and dissemination is regulated by fluctuations in cytosolic calcium concentrations, transduced in part by calcium-dependent protein kinases (CDPKs). We examined the role of CDPK2A in the lytic cycle of *Toxoplasma*, analyzing its role in the regulation of cellular processes associated with parasite motility. We used chemical-genetic approaches and conditional depletion to determine that CDPK2A contributes to the initiation of parasite motility through microneme discharge. We demonstrate that the N-terminal extension of CDPK2A is necessary for the protein's function. Conditional depletion revealed an epistatic interaction between CDPK2A and CDPK1, suggesting that the two kinases work together to mediate motility in response to certain stimuli. This signaling module appears distinct from that of CDPK3 and protein kinase G, which also control egress. CDPK2A is revealed as an important regulator of the *Toxoplasma* kinetic phase, linked to other kinases that govern this critical transition. Our work uncovers extensive interconnectedness between the signaling pathways that regulate parasite motility.

IMPORTANCE This work uncovers interactions between various signaling pathways that govern *Toxoplasma gondii* egress. Specifically, we compare the function of three canonical calcium-dependent protein kinases (CDPKs) using chemical-genetic and conditional-depletion approaches. We describe the function of a previously uncharacterized CDPK, CDPK2A, in the *Toxoplasma* lytic cycle, demonstrating that it contributes to parasite fitness through regulation of microneme discharge, gliding motility, and egress from infected host cells. Comparison of analog-sensitive kinase alleles and conditionally depleted alleles uncovered epistasis between CDPK2A and CDPK1, implying a partial functional redundancy. Understanding the topology of signaling pathways underlying key events in the parasite life cycle can aid in efforts targeting kinases for anti-parasitic therapies.

KEYWORDS CDPK, *Toxoplasma gondii*, protein kinases, calcium signaling

Apicomplexan pathogens like *Toxoplasma gondii*, *Plasmodium* spp., and *Cryptosporidium* spp. sense and adapt to changes in the host environment throughout their life cycles. Adaptation often requires rapid cellular responses, for which calcium ions (Ca^{2+}) are well suited as second messengers. Cells maintain low Ca^{2+} concentrations in the cytosol, in stark contrast to the extracellular milieu and the lumen of some organelles (1). Increased membrane permeability can therefore quickly change the cytosolic Ca^{2+} concentration and initiate signaling. In apicomplexans, such signaling controls progression through the lytic cycle.

The *Toxoplasma* lytic cycle comprises two main phases: a replicative phase during which parasites divide in a parasitophorous vacuole and a kinetic phase that includes egress from the infected host cell, gliding motility, and active invasion of a new host cell. Ca^{2+} signaling mediates the transition between the replicative and kinetic phases of

Editor L. David Sibley, Washington University School of Medicine in St. Louis, St. Louis, Missouri, USA

Address correspondence to Sebastian Lourido, lourido@wi.mit.edu.

The authors declare no conflict of interest.

See the funding table on p. 21.

Received 4 June 2023
Accepted 17 June 2023
Published 23 August 2023

the lytic cycle. After several rounds of replication, parasites actively disrupt surrounding membranes and egress from the infected cell. This process can be artificially triggered through the use of Ca^{2+} ionophores like ionomycin and A23187 (2–5) and induced indirectly through the use of phosphodiesterase inhibitors (6–9). Ca^{2+} fluxes can be observed with fluorescent dyes and genetically encoded reporters that show Ca^{2+} surges preceding gliding motility and invasion in *Toxoplasma* (5, 7, 10). Ca^{2+} oscillations also occur throughout the *Plasmodium* lytic cycle, with peaks in Ca^{2+} concentration preceding microneme secretion, invasion, gliding, and egress (11–14). Control of cytosolic Ca^{2+} concentrations is therefore critical for the regulation of the parasite lytic cycle.

Cytosolic Ca^{2+} surges originate from the release of intracellular stores or by crossing the plasma membrane (PM) from the extracellular space (15, 16). In *T. gondii*, intracellular stores include the endoplasmic reticulum (ER), acidocalcisomes, and plant-like vacuole—with the ER or a related compartment representing the most likely sources of Ca^{2+} during signaling (17). The channels responsible for Ca^{2+} release have yet to be identified in apicomplexans; however, the stimulation of the cyclic GMP (cGMP)-signaling pathway triggers this process in *T. gondii* and *Plasmodium* spp. (7, 8, 18, 19). Treatment with phosphodiesterase inhibitors (e.g., zaprinast or BIPPO) blocks hydrolysis of cGMP and can trigger egress through the release of intracellular Ca^{2+} stores (7, 20–22). Protein kinase G (PKG) is a key mediator of Ca^{2+} release, presumably through activation of phosphoinositide signaling, whereby phosphatidylinositol 4,5-bisphosphate is hydrolyzed by phosphoinositide phospholipase C into inositol triphosphate (IP_3) and diacylglycerol (DAG). This represents a potential branch point in the signaling pathway, with IP_3 triggering the release of intracellular Ca^{2+} stores through an undefined channel, while DAG is converted into phosphatidic acid and independently contributes to the kinetic phase (23). Parasite motility, therefore, requires active cGMP and Ca^{2+} pathways, consistent with the observation that stimulation by Ca^{2+} ionophores cannot overcome the inhibition of PKG in the context of egress (20).

Many Ca^{2+}-mediated phenotypes can be attributed to the Ca^{2+}-dependent discharge of micronemes, which are specialized organelles containing the adhesins necessary for gliding motility (24, 25). While synthetic treatments like ionophores, phosphodiesterase inhibitors, or alcohols can artificially raise cytosolic Ca^{2+} concentrations and trigger microneme discharge, studies suggest that serum albumin may be a natural agonist of this process (8, 26). The single-pass transmembrane protein MIC2 is a prototypical adhesin that has been used to monitor *T. gondii* microneme discharge. Following its release, MIC2 can be engaged by the actomyosin machinery for gliding motility (15, 27, 28). Several proteases rapidly process MIC2, shedding its ectodomain from the surface of the parasite—MIC2 presence in supernatants can therefore be used as a measure of microneme discharge (27). The *Plasmodium falciparum* ortholog of MIC2 is required for sporozoite motility and invasion (29), and several other adhesins are similarly released and processed in both *Toxoplasma* and *Plasmodium* (27, 30, 31). *T. gondii* micronemes additionally contain the pore-forming protein PLP1, which permeabilizes the parasitophorous vacuole membrane (PVM) and host PM during egress (32, 33). Following membrane disruption, parasites employ gliding motility to ultimately escape from the ruptured vacuole (28, 34). Perforin-like proteins are also required for the egress of *P. falciparum* and *P. berghei* merozoites and gametocytes (35–37). Although the repertoire of microneme proteins differs between species, their Ca^{2+}-dependent discharge and participation in gliding motility appear conserved across the phylum (38–40).

Ca^{2+} regulates several cellular processes besides microneme discharge, as evidenced by the wide array of proteins that respond directly to Ca^{2+} concentrations through changes in conformation, stability, localization, or interactions (9, 17, 41). Specialized domains, such as EF hands and C2 domains, endow proteins with the ability to alter their conformation in response to Ca^{2+} binding. Apicomplexans encode several EF hand–containing proteins including calmodulins (CaMs), calcineurin B, and calcium-dependent protein kinases (CDPKs). CDPKs are critical components of the Ca^{2+} signaling network due to their ability to directly respond to Ca^{2+} and phosphorylate other proteins.

Initially identified in plants, CDPKs were later found in ciliates and apicomplexans (17). Despite their similarity to Ca^{2+}/CaM–dependent protein kinases, CDPKs are absent from mammals (42). Canonical CDPKs have four C-terminal calmodulin-like EF hands, linked by an autoinhibitory domain to the kinase domain (42, 43). In plants, CDPKs control diverse stress responses, starch accumulation, cell morphology, and viability (44). Plant CDPKs vary in expression across tissue types and display diverse subcellular localizations and affinities for Ca^{2+} (43). For example, soybean CDPKα is activated by 10 times lower Ca^{2+} concentrations than CDPKγ (45, 46). Different CDPKs may therefore be tuned to respond to Ca^{2+} spikes of varying magnitudes, leading to variable downstream effects that may be further refined by subcellular localization or expression profile.

CDPKs are overrepresented in apicomplexan genomes, relative to other cytosolic kinases. There are six canonical CDPKs in *T. gondii* that can be further categorized by having short or long N-terminal extensions (42). Myristoylation sites cap the short extensions of CDPK1 and CDPK3, with an additional palmitoylation site localizing CDPK3 to the parasite PM (20, 47). By contrast, the function of the long N-terminal extensions remains unknown. A further nine CDPKs display non-canonical configurations in *T. gondii*, with varying numbers and arrangements of EF hands and additional domains (42, 48). The function of most non-canonical CDPKs remains obscure (48), with the exception of CDPK7, which has been implicated in *T. gondii* cell division and is critical for phospholipid synthesis and vesicular trafficking (49, 50). By contrast, several canonical CDPKs are required for specific life-cycle stages in apicomplexans. In *Plasmodium*, several CDPKs regulate specific steps of sexual differentiation (51, 52).

CDPKs are critical for kinetic-phase phenotypes in *Toxoplasma* and *Plasmodium*, including microneme discharge, gliding motility, invasion, and egress. TgCDPK1 and TgCDPK3 control *Toxoplasma* egress downstream of PKG (20, 47, 53), analogously to PfCDPK5 in *Plasmodium* (13, 54). In *Toxoplasma*, CDPK1 is additionally required for invasion, potentially due to its regulation of microneme secretion under a broader array of conditions than CDPK3 (20, 53). Altogether, CDPKs have been revealed as essential components of the apicomplexan Ca^{2+}-signaling network, although the functions of many individual kinases remain unexplored.

In reviewing the results of a genome-wide essentiality screen, most canonical CDPKs were dispensable in tachyzoites; however, CDPK2A has remained uncharacterized despite its impact on parasite fitness (55). We sought to characterize the function of CDPK2A within the lytic cycle, comparing its role to that of CDPK1 and CDPK3, two previously described regulators of the kinetic phase. Through a combination of chemical and genetic manipulations, we uncover significant functional overlap between the pathways controlled by different CDPKs and associated pathways, providing new insights into the regulation of the *T. gondii* kinetic phase.

RESULTS

Chemical-genetic analysis of CDPK2A demonstrates its involvement in parasite egress

To identify the CDPKs that are necessary during the parasite lytic cycle, we examined the results of a genome-wide knockout screen that measured the relative contribution of each gene to fitness as parasites replicated in human fibroblasts (55). Most canonical CDPKs were dispensable in this analysis, including the previously studied CDPK3; however, CDPK1 and CDPK2A were fitness-conferring, indicated by phenotype scores of −3.3 and −2.05, respectively (Fig. 1A). Of these potentially essential CDPKs, the function of CDPK2A has not been previously examined. Studies of CDPK1 and CDPK3 used analog-sensitive kinase alleles, in which the gatekeeper residue of the ATP-binding pocket of the kinase of interest is mutated to Gly, yielding a binding pocket that accommodates bulky ATP-analog inhibitors—also known as bumped kinase inhibitors—like 1-(tert-butyl)-3-(3-methylbenzyl)-1H-pyrazolo[3,4-d]pyrimidin-4-amine (3-MB-PP1) (Fig. 1B) (56–58). CDPK1 has a naturally occurring Gly gatekeeper and can be rendered resistant to 3-MB-PP1 inhibition through mutation of the gatekeeper residue to Met—

the same residue that renders CDPK3 and CDPK2A naturally resistant to the inhibitor (56, 57). Comparison of analog-sensitive and insensitive alleles can be used to isolate the effect of inhibiting the kinase in question. Using this approach, CDPK1 was shown to control parasites' ability to move, invade, and egress from host cells (53). By contrast, compound-mediated inhibition of CDPK3 determined its contribution to motility and egress in response to specific agonists, but not invasion (20), corroborating genetic studies (47, 59).

Given the apparent fitness contribution of CDPK2A, we sought to examine its role in the *Toxoplasma* lytic cycle through the use of analog-sensitive alleles. In a strain harboring a 3-MB-PP1-resistant, myc-tagged CDPK1 allele ($CDPK1^{M}$) (20), we modified the CDPK2A locus to introduce a C-terminal Ty epitope tag and either a Met or Gly gatekeeper residue (Fig. 1C). The Met modification ($CDPK2A^{M}$) retains the natural resistance of CDPK2A to 3-MB-PP1, whereas the Gly modification ($CDPK2A^{G}$) renders the kinase 3-MB-PP1 sensitive. We confirmed the presence of the mutated gatekeeper residues by allele-specific PCR (Fig. S1A) and the expression of the Ty-tagged CDPK2A alleles by immunoblot (Fig. 1D). Construction of the isogenic strains carrying alleles of CDPK2A with different susceptibilities to bumped kinase inhibitors allowed us to examine the effect of kinase inhibition on various steps within the lytic cycle.

Parasites can be stimulated to egress from host cells by treating cultures with the Ca^{2+} ionophore A23187 (2) or phosphodiesterase inhibitors such as zaprinast (20) or BIPPO (22). Different agonists have been used to identify pathway-specific requirements for certain kinases (20, 60). Egress leads to loss of host-cell integrity, which can be assayed quantitatively and kinetically as the incorporation of the fluorescent dye DAPI (4′,6-diamidino-2-phenylindole) into the nuclei of permeabilized cells or by measuring the release of lactate dehydrogenase (LDH) from permeabilized host cells (61, 62).

We compared the impact of inhibiting CDPK1, CDPK3, or CDPK2A on A23187-stimulated egress by quantifying DAPI-stained host nuclei over time. All three kinases appeared to be required for egress under these conditions. Inhibition of either $CDPK1^{G}$ or $CDPK3^{G}$ strains reduced egress by 66% or 84%, respectively, in agreement with previous findings (20, 47, 53, 59). Analogously, inhibition of $CDPK2A^{G}$ decreased egress by 61% compared to vehicle treatment (Fig. 1E and F). Importantly, parasites expressing the resistant allele ($CDPK2A^{M}$) egressed normally in the presence of 3-MB-PP1. To compare the rates of egress, we determined the time required for each strain to achieve half of the maximum egress observed for the respective vehicle-treated control ($T_{half\text{-}max}$). Inhibition of all three kinases prevented parasites from reaching half of the maximum egress during the 10-minute observation period (denoted as $T_{half\text{-}max}$ >600 seconds; Fig. S1B). To ensure that the effects observed were the result of differences in egress and not the multiplicity of infection, we verified that monolayers had equivalent numbers of parasite vacuoles (Fig. S1C). Since the kinetic assays are performed at a single dose of the inhibitor, we used the endpoint LDH assay to examine the inhibition of egress in these strains across a range of 3-MB-PP1 concentrations. While $CDPK2A^{M}$ and $CDPK3^{M}$ parasites were resistant to all the 3-MB-PP1 concentrations tested (up to 5 µM), egress of $CDPK2A^{G}$ parasites was inhibited with an EC_{50} of 1.7 nM, below the 47.5 nM EC_{50} calculated for $CDPK3^{G}$ (Fig. S1D and E). The EC_{50} of 3-MB-PP1 against $CDPK1^{G}$ was below 1 µM in previous studies (20). Taken together, these results suggest that CDPK2A contributes to egress, along with CDPK1 and CDPK3.

We next assessed the contribution of CDPK2A to parasite egress after treatment with the phosphodiesterase inhibitor zaprinast. Inhibition of CDPK2A or CDPK1 caused a significant reduction in egress (Fig. 1G and H). By contrast, CDPK3 inhibition simply delayed egress ($T_{half\text{-}max}$ of 257 seconds versus 117 seconds for vehicle-treated parasites), with parasites eventually reaching levels of egress equivalent to $CDPK3^{M}$ (Fig. 1G and H; Fig. S1F). These differences were attributable to egress because similar numbers of vacuoles were present in all samples (Fig. S1G). The findings are consistent with previous work suggesting that PKG activation, through inhibition of the cGMP-degrading phosphodiesterases, can compensate for the inhibition of CDPK3 (20, 60).

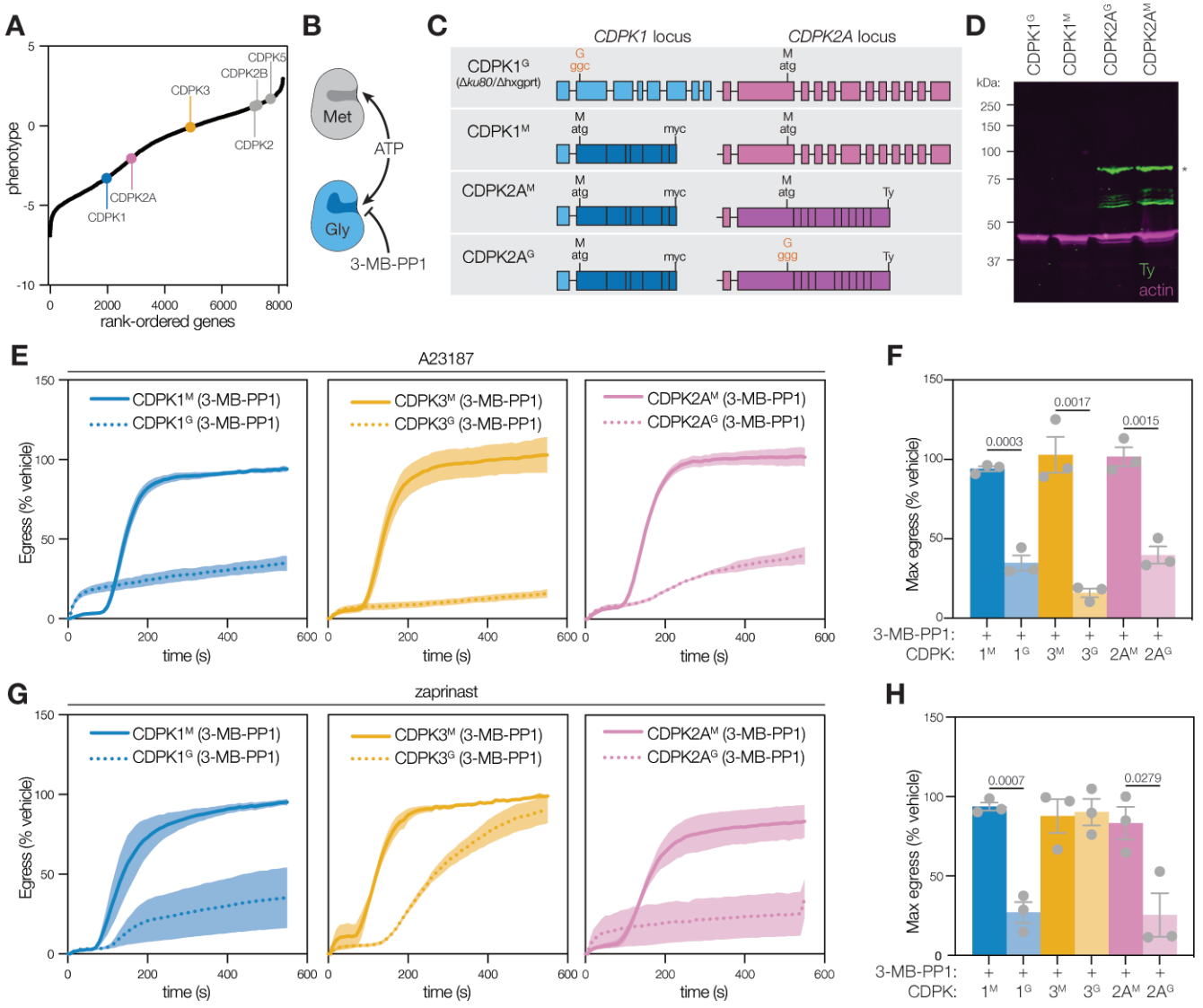

FIG 1 CDPK2A is required for stimulated parasite egress in addition to CDPK1 and CDPK3. (A) *Toxoplasma* genes are ranked by their phenotype, as determined in a genome-wide knockout screen (55). Points represent the mean phenotype score of $n = 4$ replicates. Six canonical calcium-dependent protein kinases are highlighted, including CDPK1 (blue), CDPK3 (yellow), and CDPK2A (pink). (B) Schematic representation of chemical-genetics strategy. The gatekeeper residue of a kinase of interest is mutated, with minimal impact on ATP binding but altered binding of bulky ATP-mimetic inhibitors (e.g., 3-MB-PP1) depending on the size of the binding pocket. (C) Schematic representation of CDPK1 and CDPK2A loci in the analog-sensitive (AS) kinase strains. Darker shading indicates synthetic DNA. 3-MB-PP1-sensitive alleles are highlighted in red. (D) Immunoblot of wild-type ($CDPK1^G$), parental ($CDPK1^M$), and Ty-tagged CDPK2A AS kinase strains shows the expression of the tagged kinase; ACT1 (actin) is used as a loading control; asterisk indicates the approximate molecular weight of full-length CDPK2A. (E) Kinetic traces of A23187-stimulated parasite egress. Graphs are egress of 3-MB-PP1-treated parasites as percentage of the vehicle. A23187 was added 1 second after the start of imaging. Line plots represent the mean ± SEM for $n = 3$ biological replicates. (F) Maximum egress achieved by each strain during the 10-minute observation window, displayed as percentage of the vehicle. Bars represent the mean ± SEM of $n = 3$ biological replicates; significance was calculated by unpaired *t*-test. (G) Kinetic traces of zaprinast-stimulated parasite egress. Graphs are egress of 3-MB-PP1-treated parasites as percentage of the vehicle. Zaprinast was added 1 second after the start of imaging. Line plots represent the mean ± SEM for $n = 3$ biological replicates. (H) Maximum egress was achieved by each strain during the 10-minute observation window, displayed as percentage of the vehicle. Bars represent the mean ± SEM of $n = 3$ biological replicates; significance was calculated by unpaired *t*-test.

The N-terminal extension of CDPK2A impacts its localization and function

CDPK2A has a long N-terminal extension, which is absent from CDPK1 and CDPK3 (42). We examined whether the N-terminal extension is required for CDPK2A function. Attempts to amplify the 5′ end of *CDPK2A* from cDNA yielded two isoforms, which

were used to clone two complementation constructs expressed under the heterologous *SAG1* promoter. Complement 1 (c.1) and complement 2 (c.2) differ in how much of the N-terminal extension they include due to alternative splicing; however, both constructs contain the entire kinase domain (Fig. 2A). We also generated complement 3 (c.3), which included 1.5 kb of sequence upstream of the predicted translational start site, as well as the full first intron, enabling both isoforms to be expressed under endogenous regulation. Complementing alleles had Met gatekeepers and C-terminal hemagglutinin (HA) tags and were expressed from a second locus in CDPK2A^{G} parasites (Fig. 2A; Fig. S2A). This strategy enables inhibition of the endogenous CDPK2A^{G} to assess the function of the second copy. The selected clones exhibited comparable levels of CDPK2A^{M} expression (Fig. 2B). We found that endogenously tagged CDPK2A (Ty) localizes to the periphery of intracellular parasites, possibly to the inner membrane complex or PM (Fig. 2C). Out of the three complementing vectors, only c.3, which retained the endogenous 5′ end of the *CDPK2A* mRNA, localized to the parasite periphery, similarly to the endogenous copy. By contrast, c.1 and c.2 localized to the parasite cytosol (Fig. 2C). This suggested that localization to the parasite periphery is dependent on the endogenous 5′ end of the gene, though not necessarily the presence of the N-terminal extension, perhaps due to a cryptic alternative start site or a requirement for precise timing of expression.

We next assessed the function of the complementing alleles. We inhibited the endogenous CDPK2A^{G} allele and assessed whether each of the complemented strains could egress following A23187 or zaprinast induction. With A23187 stimulation, c.1 and c.3 strains egressed normally despite inhibition of the endogenous allele; however, inhibitor-treated c.2 parasites exhibited no complementation (Fig. 2D and E). The two alleles that did complement (c.1 and c.3) egressed with kinetics comparable to 3-MB-PP1-resistant CDPK2A^{M} parasites, reaching half the maximal egress around 200 seconds (Fig. S2B). We confirmed that in all cases the monolayers were equivalently infected (Fig. S2C). Complementation during zaprinast-induced egress was intermediate but followed similar trends, with c.3 achieving 75% as much egress as vehicle-treated lines and c.1 egressing to 60% of vehicle, while there was no apparent complementation by c.2 (Fig. 2F and G). This partial rescue was also reflected in the rates of egress (Fig. S2D and E). These findings suggest that the N-terminal extension of CDPK2A—present in c.1 and c.3 constructs but absent in c.2—is required for parasite egress. It seems that c.1 and c.3 are both able to functionally complement for the inhibited endogenous allele, despite their different localizations.

Conditional depletion of CDPK2A only partially mimics chemical inhibition

Off-target effects of 3-MB-PP1 interfere with the chemical-genetic approach described above during long-term culture, making it challenging to assess the impact of kinase inhibition over several lytic cycles (63). Auxin-inducible degradation of target proteins has been adapted to *Toxoplasma* and used to investigate protein kinases and associated signaling pathways (64, 65). We employed this conditional-depletion system as an orthogonal strategy to assess the CDPK function. Briefly, a protein of interest is tagged with an AID in a strain expressing TIR1. When transgenic parasites are treated with the plant hormone auxin—most commonly indolacetic acid (IAA)—the tagged protein is ubiquitinated and targeted by the proteasome for degradation (66) (Fig. 3A). Protein depletion occurs within minutes to hours in *Toxoplasma*, depending on the protein of interest (64, 65). We generated a panel of strains in which CDPK1, CDPK3, or CDPK2A were tagged at their C-termini with the Ty epitope followed by mNeonGreen and a minimal AID (Fig. S3A). Localization of CDPK2A-AID was consistent with the chemical-genetic alleles, with mNeonGreen signal observed at the parasite periphery (Fig. 3B). Expression of all mNeonGreen-tagged alleles was measured by FACS in parasites with and without IAA treatment. Three hours of IAA treatment was sufficient to observe robust and uniform depletion of each CDPK (Fig. 3C). Based on these results, we treated

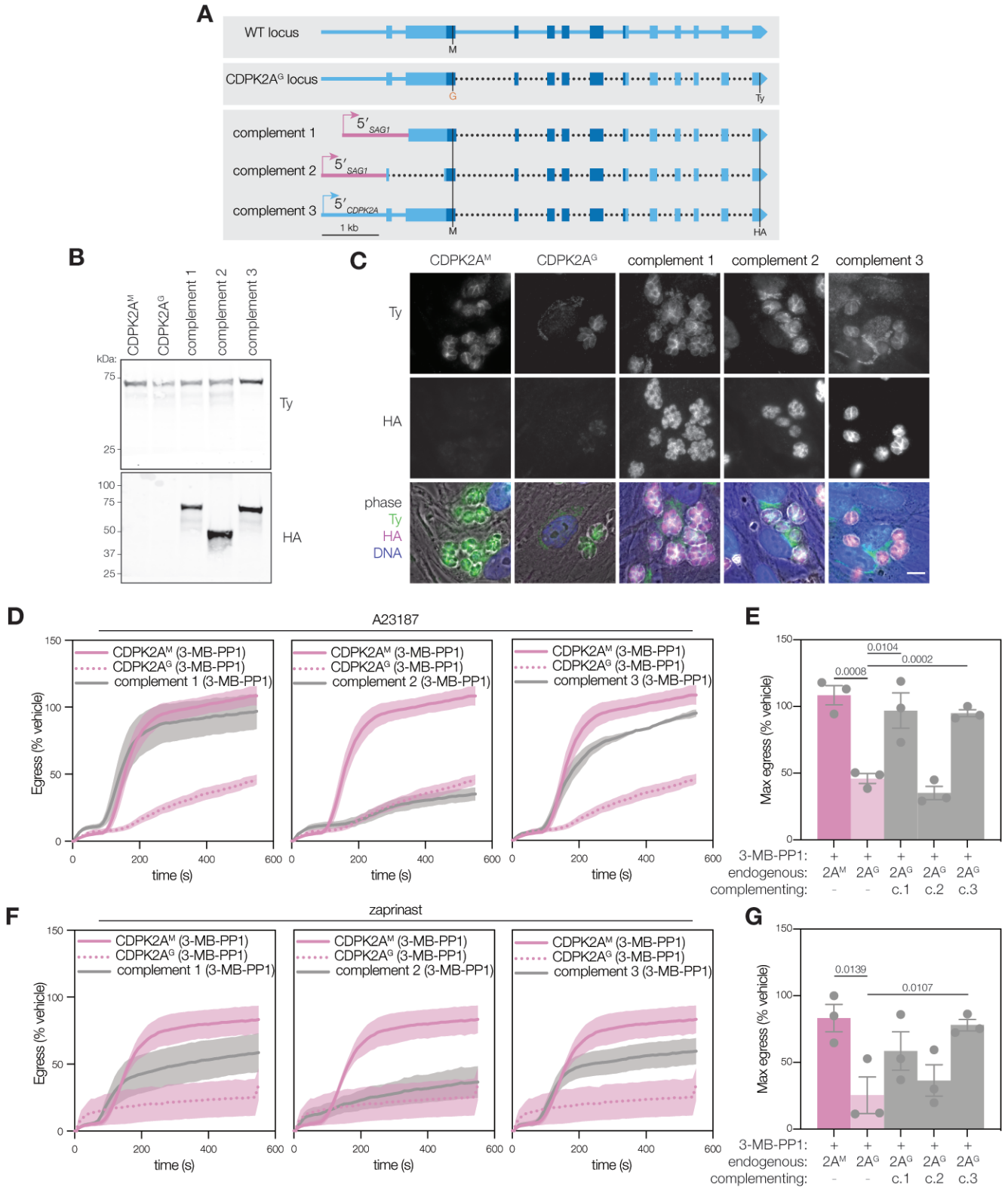

FIG 2 The N-terminal extension of CDPK2A influences its localization and is necessary for parasite egress. (A) Schematic representation of complementing constructs with comparison to CDPK2A genomic locus. Dotted lines indicate gaps in the sequence where introns have been removed. Shaded region encoding the kinase domain. 3-MB-PP1-sensitive alleles are highlighted in red. (B) Immunoblot of complemented strains probing for the endogenous allele with Ty and the complementing allele with HA. (C) Immunofluorescence microscopy of endogenously Ty-tagged CDPK2A^{M} and CDPK2A^{G} and HA-tagged complementing copies

(Continued on next page)

FIG 2 (Continued)

of CDPK2A^{M}. Merged image displays Ty (green), HA (magenta), DNA (blue), and phase (gray scale). Scale bar is 10 µm. (D) Kinetic traces of A23187-stimulated parasite egress. Graphs are egress of 3-MB-PP1-treated parasites as percentage of the vehicle. A23187 was added 1 second after the start of imaging. Line plots represent mean ± SEM for n = 3 biological replicates. (E) Maximum egress achieved by each strain during the observation window, displayed as percentage of the vehicle. Bars represent mean ± SEM of n = 3 biological replicates; significance was calculated by unpaired one-tailed t-test. (F) Kinetic traces of zaprinast-stimulated parasite egress. Graphs are egress of 3-MB-PP1-treated parasites as percentage of the vehicle. Zaprinast was added 1 second after the start of imaging. Line plots represent mean ± SEM for n = 3 biological replicates. (G) Maximum egress was achieved by each strain during the observation window, displayed as percentage of the vehicle. Bars represent the mean ± SEM of n = 3 biological replicates; significance was calculated by unpaired one-tailed t-test.

the parasites with auxin for a minimum of 3 hours for downstream analyses, achieving kinase degradation within less than a single cell cycle.

We assessed egress following the acute depletion of CDPK1, CDPK3, or CDPK2A. Stimulation with A23187 induced minimal egress in CDPK-depleted parasites, indicating that all three kinases are necessary for egress under these conditions (Fig. 3D and E); this is consistent with our chemical-genetic approach. Analysis of egress kinetics showed that all three depleted lines failed to egress normally within the observation window, in contrast to the TIR1 parental parasites (Fig. S3B and C).

We next assessed the ability of CDPK-depleted parasites to egress in response to zaprinast stimulation. Depletion of CDPK1 or CDPK3 phenocopied their chemical-genetic inhibition. CDPK1-depleted parasites were unable to egress, whereas CDPK3-depleted parasites displayed delayed but near-complete egress (Fig. 3F and G; Fig. S3D). Surprisingly, CDPK2A-depleted parasites achieved normal levels of egress (90% of vehicle-treated parasites), albeit with a delay ($T_{half\text{-}max}$ of 230 seconds, compared to 120 seconds for the parental TIR1 strain), despite equivalent levels of overall infection (Fig. 3F and G; Fig. S3D and E). We conclude that differences between the strains used for chemical inhibition or depletion render CDPK2A differentially required for egress. Such differences could result from the manipulation of the *CDPK2A* locus or the strain background in which the mutants were generated.

Inhibition of CDPK1 reveals epistasis with CDPK2A

We considered whether differences in the CDPK1 alleles of the parental lines could lead to the differential requirement for CDPK2A in zaprinast-stimulated egress when assessed by either approach. CDPK1^{M} was used for chemical genetics while conditional-depletion strains harbor the wild-type CDPK1^{G} allele. Enzyme assays have demonstrated that CDPK1^{G} is more catalytically active than CDPK1^{M}, although either allele can support parasite replication (67). Based on the presence of CDPK1^{M} in the AS kinase lines and the similar phenotypes of CDPK1 and CDPK2A, we hypothesized that partial loss of CDPK1 activity could increase reliance on CDPK2A for egress.

We assessed whether CDPK1 and CDPK2A exhibit epistasis by broadly examining the lytic cycle during plaque formation. We partially inhibited CDPK1 with a sublethal concentration of 3-MB-PP1 in the context of CDPK2A expression or depletion, using the CDPK2A-AID strain. CDPK2A-depleted parasites failed to form plaques when CDPK1 was partially inhibited. By contrast, plaquing was not impacted by the partial inhibition of CDPK1 in the context of CDPK3 depletion (Fig. 4A). This suggests that the requirement for CDPK2A during the lytic cycle depends on the level of CDPK1 activity.

We next examined the epistatic interaction between the two kinases during zaprinast-stimulated egress using endpoint assays. Treating parasites with a range of 3-MB-PP1 concentrations to inhibit CDPK1^{G}, we observed that CDPK2A depletion renders parasites hypersensitive to CDPK1 inhibition (Fig. 4B; Fig. S4). By contrast, depletion of CDPK3 did not change the sensitivity of parasites to CDPK1 inhibition by 3-MB-PP1. An F-test was used to determine whether IAA-treated and -untreated samples could be modeled with a single curve. CDPK2A-AID data points did not fit a single curve (P < 0.0001), whereas TIR1 and CDPK3-AID data points follow a single curve (ns). This observation is supported by the calculated EC_{50} for 3-MB-PP1, which decreases significantly when CDPK2A-AID parasites are treated with auxin (Fig. 4C). The

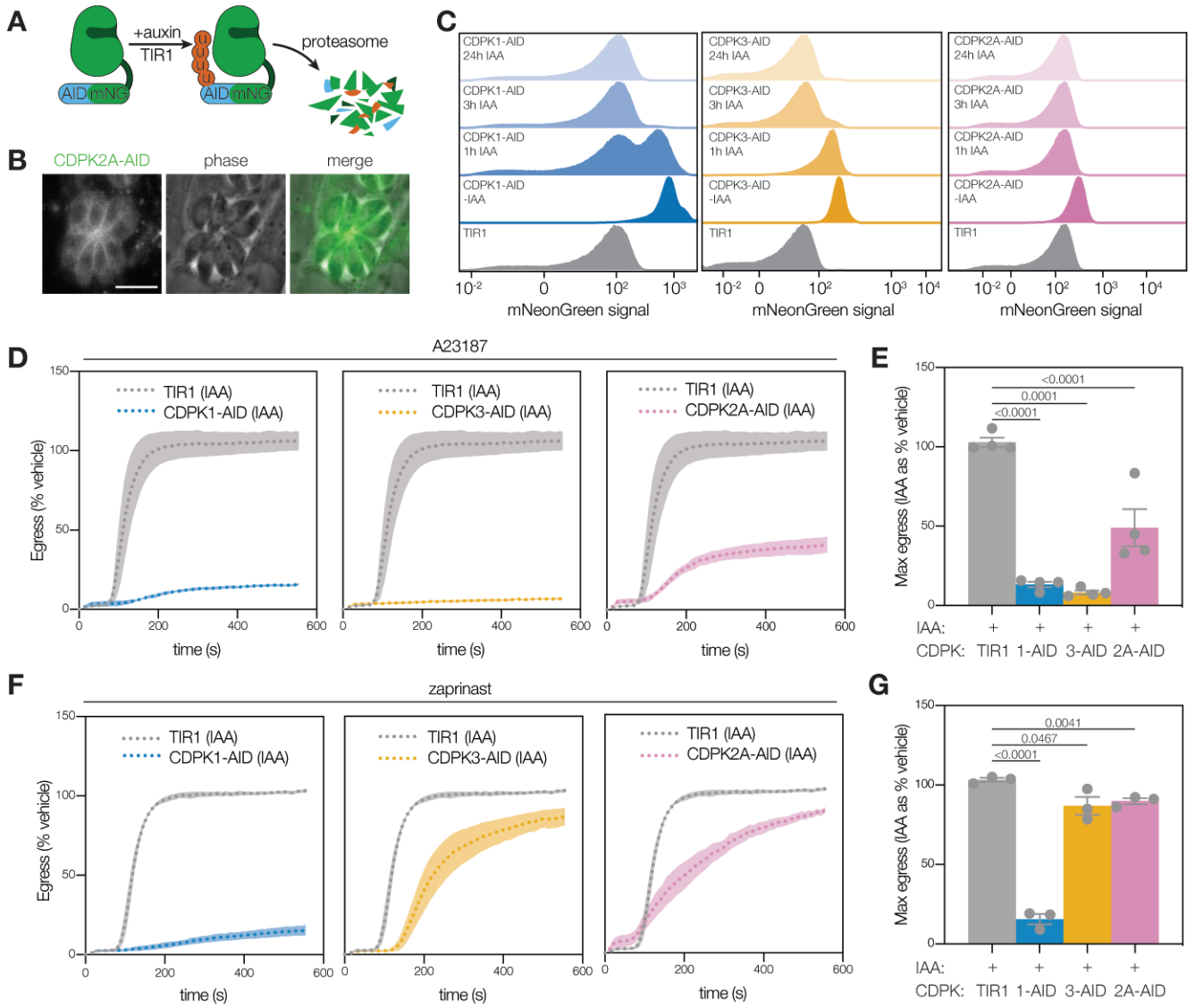

FIG 3 Conditional depletion of CDPKs reveals CDPK2A is required for A23187-stimulated egress, but not for zaprinast-stimulated egress. (A) Schematic representation of a CDPK tagged with a minimal auxin-inducible degron (AID), Ty, and mNeonGreen. When IAA is added, the TIR1 ubiquitin ligase complex is recruited to the tagged protein and targets it for proteasomal degradation. (B) Live-cell imaging of CDPK2A-AID parasites shows the mNeonGreen signal concentrated at the parasite periphery. Scale bar is 10 µm. (C) FACS analysis of mNeonGreen-tagged CDPK-AID parasites and TIR1 parental line with and without the addition of auxin (IAA) shows the expression of the mNeonGreen fusion and kinetics of auxin-induced depletion. (D) Kinetic traces of A23187-stimulated parasite egress. Graphs are egress of IAA-treated parasites as percentage of the vehicle. A23187 was added 1 second after the start of imaging. Line plots represent mean ± SEM for $n = 4$ biological replicates. (E) Maximum egress achieved by each strain during the observation window, displayed as percentage of the vehicle. Bars represent mean ± SEM of $n = 4$ biological replicates; significance was calculated by unpaired *t*-test. (F) Kinetic traces of zaprinast-stimulated parasite egress. Graphs are egress of IAA-treated parasites as percentage of the vehicle. Zaprinast was added 1 second after the start of imaging. Line plots represent the mean for $n = 3$ biological replicates with error bands representing SEM. (G) Maximum egress achieved by each strain during the observation window, displayed as percentage of the vehicle. Bars represent the mean ± SEM of $n = 3$ biological replicates; significance calculated by the unpaired *t*-test.

combination of chemical inhibition and protein knockdown allowed us to demonstrate that CDPK2A becomes more critical for egress when CDPK1 activity is compromised due to a mutant gatekeeper allele, as in CDPK1^{M}, or upon chemical inhibition. We surmise that the AID-tagged lines more closely reflect physiological conditions—with a wildtype CDPK1 allele—than AS kinase lines, so we examined the function of CDPK2A across the lytic cycle using conditional depletion.

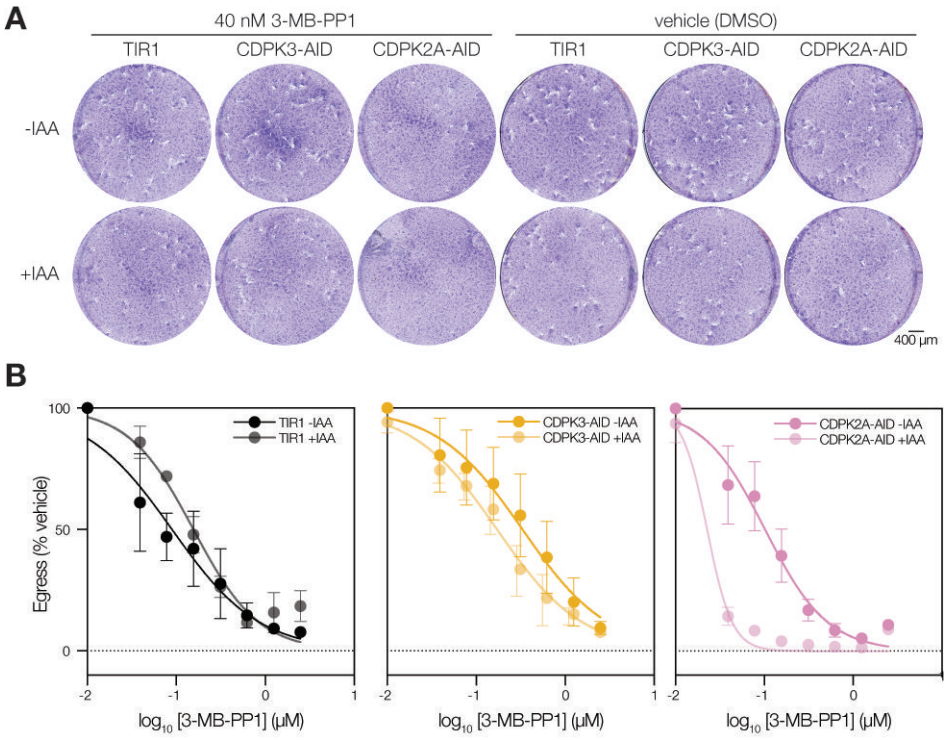

C

	-IAA EC_{50} (µM) (mean ± SEM)	+IAA EC_{50} (µM) (mean ± SEM)	*p*-value
TIR1	0.12 ± 0.049	0.16 ± 0.018	0.2541
CDPK3-AID	0.46 ± 0.25	0.21 ± 0.084	0.1954
CDPK2A-AID	0.12 ± 0.039	0.023 ± 0.0034	0.0370

FIG 4 CDPK1 and CDPK2A comprise a signaling module that regulates zaprinast-stimulated egress and the lytic cycle. (A) Partial inhibition of endogenous $CDPK1^G$ by 3-MB-PP1 (40 nM) leads to ablation of plaque formation by parasites conditionally depleted of CDPK2A. Scale bar is 400 µm. (B) Dose-response of CDPK1 inhibition with 3-MB-PP1 monitoring endpoint zaprinast-stimulated egress in parasites depleted of or expressing the indicated CDPK. Graphs are egress of IAA-treated parasites as percentage of the vehicle. Mean ± SEM plotted for $n = 3$ biological replicates. (C) EC_{50} (µM) for 3-MB-PP1 of CDPK-depleted or untreated parasites; significance was calculated by unpaired one-tailed *t*-test across $n = 3$ biological replicates.

Conditional depletion reveals a role for CDPK2A at various stages of the lytic cycle

Plaque formation results from repeated cycles of host cell lysis. As expected, the depletion of CDPK1 blocked plaque formation (53), whereas CDPK3 appeared dispensable for the process (47, 55, 59). By comparison, the depletion of CDPK2A reduced the number and size of plaques (Fig. 5A and B; Fig. S5A and B). Even without IAA, CDPK2A-AID parasites formed smaller plaques than the parental line, suggesting that AID tagging of the kinase may partially compromise its function. These results are in line with the phenotype scores in the genome-wide fitness screen (55), placing CDPK2A at an intermediate fitness contribution, between CDPK1 and CDPK3.

To assess whether a smaller epitope would relieve the impact of tagging on CDPK2A, we generated a conditional knockdown strain in which the AID tag was fused to HA instead of mNeonGreen (CDPK2A-AID-HA; Fig. S5C and D). CDPK2A-AID-HA-tagged parasites also formed smaller plaques than the TIR1 parental line, but the defect was not as pronounced as that of CDPK2A-AID. As anticipated, the depletion of the kinase further reduced plaque size (Fig. S5E). To measure the fitness cost associated with tagging and depleting CDPK2A, we performed competition assays against a wild-type strain (Fig.

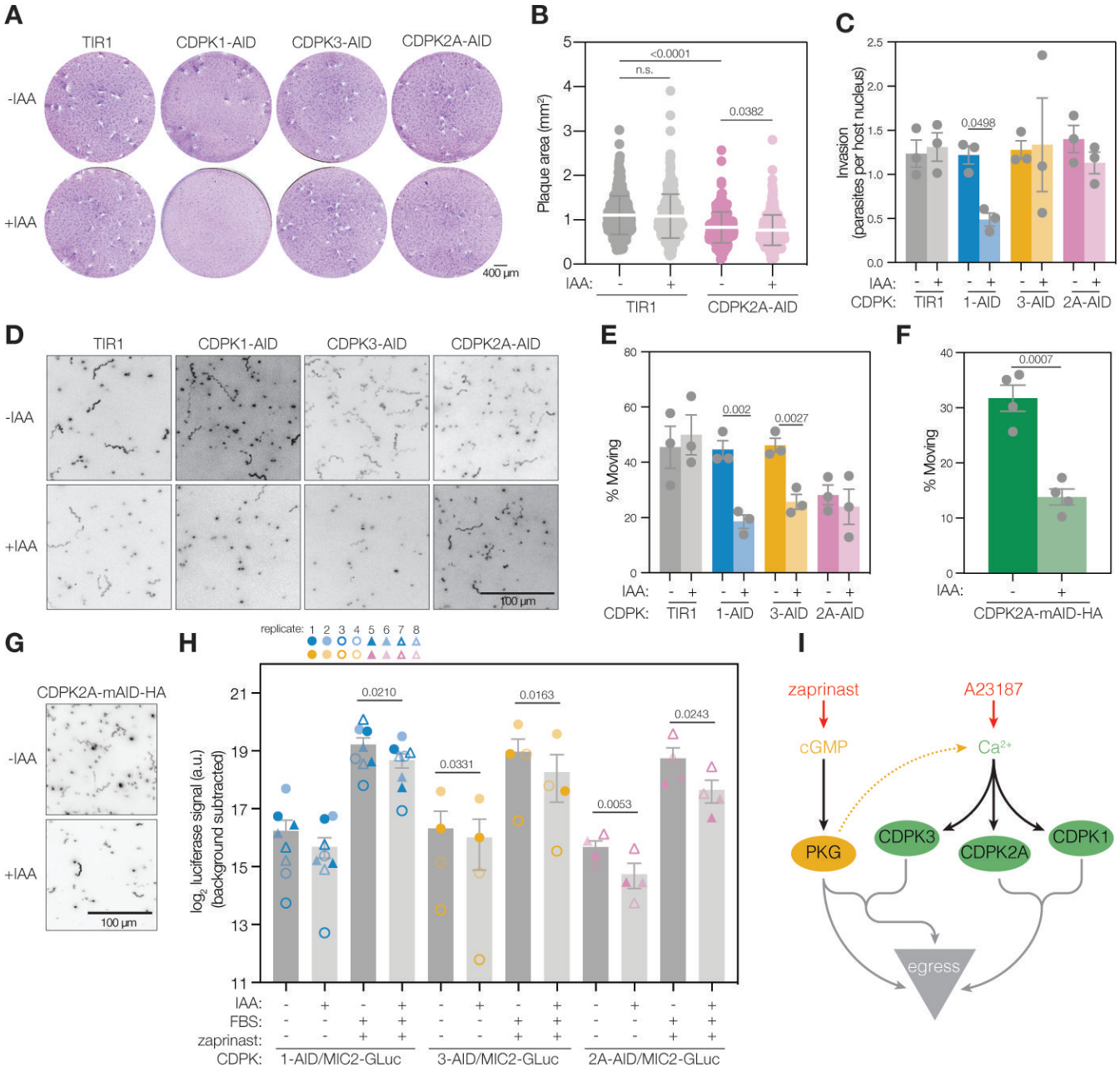

FIG 5 CDPK2A impacts plaque formation, gliding motility, and microneme discharge. (A) Depletion of each of the three CDPKs affected plaque formation differently: parasites depleted of CDPK1 formed no plaques, those depleted of CDPK2A formed fewer plaques, and those depleted of CDPK3 plaqued normally. Images are representative of $n = 4$ biological replicates. Scale bar is 400 µm. (B) CDPK2A-AID parasites form smaller plaques than the TIR1 parental line, and the effect is exacerbated by the depletion of the kinase (+ IAA). Scatter plot displays areas for >270 individual plaques per sample; mean ± SD is overlaid; *P*-value was calculated by unpaired *t*-test. (C) CDPK2A depletion does not impact parasites' ability to invade host cells. Bars represent the mean ± SEM for $n = 3$ biological replicates; *P*-value calculated by paired *t*-test. (D) 3D gliding motility in Matrigel following the depletion of each kinase. Maximum intensity projections of tracked parasites. Scale bar is 100 µm. (E) Proportion of parasites observed moving in 3D gliding motility assays. Each point is the mean of three technical replicates with 634–1,500 observations per condition; bars represent the mean ± SEM of $n = 3$ biological replicates; significance was calculated by unpaired one-tailed *t*-test. (F) Proportion of parasites observed moving in 3D gliding motility assays of CDPK2A-AID-HA parasites with and without IAA. Each point is the mean of the technical replicates; bars represent the mean ± SEM of $n = 4$ biological replicates; significance was calculated by paired *t*-test. (G) 3D gliding motility in Matrigel following the depletion of CDPK2A-AID-HA. Maximum intensity projections of tracked parasites. Scale bar is 100 µm. (H) Depletion of CDPKs decreases microneme discharge. *Gaussia* luciferase activity, from a microneme-localized construct, was assayed in supernatants following 30 minutes of stimulation with FBS and zaprinast. Points represent individual biological replicates ($n = 8$ for CDPK1-AID, $n = 4$ for CDPK3-AID or CDPK2A-AID), with bars indicating mean ± SEM; significance was calculated by paired one-tailed *t*-test. (I) Proposed model for the relationship between kinases that positively regulate parasite motility.

S5F). CDPK2A-AID and CDPK2A-AID-HA parasites were outcompeted by wild-type parasites (TIR1/IMC1-TdTom), and depletion of CDPK2A further decreased the fitness of either tagged strain. In contrast, the abundance of CDPK3-AID parasites remained relatively stable in competition with wild type, and depletion of the kinase did not impact fitness significantly. While the smaller epitope tag still appears to impact CDPK2A function, it serves to corroborate the phenotypes associated with CDPK2A, including the egress delay associated with its depletion (Fig. S5G and H).

The impact of CDPK2A depletion on plaquing efficiency and survival may result from impaired or inefficient invasion, slower replication, decreased motility, or a combination of factors that must be deconvoluted through single-phenotype assays. We assessed whether CDPK2A is required for parasite invasion of host cells using an immunofluorescence assay that distinguishes between invaded and extracellular parasites. As expected, depletion of CDPK1 blocked parasite invasion, whereas depletion of CDPK3 had no effect (20, 47, 53). As with CDPK3, depletion of CDPK2A did not affect parasite invasion (Fig. 5C). The dispensability of CDPK2A for the invasion was corroborated by chemical genetics. Inhibition of AS CDPK1 blocked invasion, while inhibition of CDPK2A had no impact on this process (Fig. S6A).

Gliding motility is necessary for parasite egress from host cells and invasion (68). We quantitatively assessed the 3D motility of CDPK-depleted parasites in Matrigel, which captures motility defects that are hard to appreciate by traditional 2D motility assays (69). Depletion of CDPK1 or CDPK3 decreased the proportion of parasites moving during the assay by 58% or 44%, respectively (Fig. 5D and E). A smaller fraction of the CDPK2A-AID parasites was motile compared to the parental TIR1 strain, perhaps reflecting the hypomorphic behavior of the tagged allele; however, the proportion of CDPK2A-AID parasites moving was not decreased further by pre-treatment with IAA (Fig. 5E). Besides the proportion of parasites moving, other aspects of gliding motility appeared largely unchanged by the downregulation of any of the CDPKs, with the exception of decreased track length and displacement on downregulation of CDPK1. Speed of motility was comparable between moving parasites from all strains (Fig. S6B through E).

To confidently identify differences in the motility of the TIR1 parental and CDPK2A-AID strains, we compared them directly. Indeed, AID tagging of CDPK2A decreased the proportion of parasites moving in the assay (Fig. S6F). Tagging with HA instead of mNeonGreen (CDPK2A-AID-HA) generated parasites with rates of motility indistinguishable from wild type in terms of the proportion moving (Fig. S6G). We therefore measured the effect of depleting CDPK2A in this context. Comparison of CDPK2A-AID-HA motility following pre-treatment with IAA or vehicle revealed a 56% decrease in the proportion of parasites moving when CDPK2A was depleted (Fig. 5F and G). We also observed a significant decrease in track length, but speed appeared unchanged (Fig. S6H through K)—a trend that was observed but had not reached significance for CDPK2A-AID (Fig. S6B). These results suggest that CDPK2A plays a critical role in gliding motility and confirm the previously reported roles for CDPK1 and CDPK3 (20, 47, 53, 59, 70).

We also assessed the ability of CDPK2A-depleted parasites to secrete micronemal contents. We expressed *Gaussia* luciferase (GLuc) fused to myc-tagged MIC2 in CDPK-AID transgenic lines to quantify microneme protein secretion following knockdown of each kinase (Fig. S6L) (8). Following CDPK depletion, parasites were stimulated to secrete with FBS and zaprinast. Microneme discharge was measured based on the luciferase signal present in the ESA fraction. Depletion of CDPK1, CDPK3, or CDPK2A decreased microneme discharge following stimulation with FBS and zaprinast for 30 minutes (Fig. 5H). Interestingly, CDPK2A depletion did not significantly decrease MIC2 secretion at an acute 5-minute time point, although the impact of CDPK1 and CDPK3 was still evident (Fig. S6M). We further verified that basal MIC2 levels were equivalent between strains and that CDPK depletion does not impact total MIC2 in parasite lysates (Fig. S6N). Due to the compressed dynamic range of the quantitative assays, we confirmed that CDPK1 and CDPK2A participate in microneme discharge using conventional MIC2 secretion assays. Parasites were stimulated with FBS and ethanol (26, 71), ESAs were collected

after 15 minutes, and MIC2 release was analyzed by immunoblot. We observed a robust decrease in the amount of MIC2 secreted by parasites depleted of CDPK1 or CDPK2A (Fig. S6O and P). Overall, these results indicate CDPK1, CDPK3, and CDPK2A are all involved in microneme protein secretion, but possibly to varying degrees or with different kinetics.

DISCUSSION

We examined the role of CDPK2A in the lytic cycle of *Toxoplasma*. Using a combination of chemical-genetic and conditional depletion methods, we show that CDPK2A contributes to the initiation of parasite egress through microneme discharge and gliding motility. We further demonstrated that the N-terminal extension of CDPK2A is necessary for the protein's function in egress. Contrasting results from chemical inhibition and conditional depletion revealed an epistatic interaction between CDPK2A and CDPK1. Our results suggest that CDPK2A and CDPK1 work together to mediate egress following the stimulation of the PKG pathway (Fig. 5I). This signaling module might be differentially compartmentalized from CDPK3 and PKG, which localize to the PM. Our work uncovered additional complexity and interconnectedness in the signaling pathways that govern key events during the parasite lytic cycle.

CDPK2A contributes to overall parasite fitness. Plaque assays showed limited growth for parasites depleted of CDPK2A—an intermediate effect between the dispensable CDPK3 and the essential CDPK1. We further demonstrated that CDPK2A-depleted parasites are outcompeted by wild type in mixed cultures, while CDPK3-depleted parasites are not. These observations are consistent with previous genome-wide loss-of-function screens, which calculated a phenotype for CDPK2A intermediate between CDPK1 and CDPK3 (55). We have sought to determine what differentiates the fitness-conferring CDPK1 and CDPK2A from the dispensable CDPK3. Chemical-genetic approaches previously showed that accumulation of cGMP, which activates PKG, can compensate for the loss of CDPK3 during egress (20). The reliance on CDPK2A similarly appeared to be conditional on the activity of other kinases. While all three CDPKs studied were required for egress in response to Ca^{2+} ionophores, conditional depletion of CDPK2A could be partially compensated through hyperstimulation of the PKG pathway, as was previously observed for CDPK3 (20). However, unlike CDPK3, compensation for CDPK2A loss depended on the level of CDPK1 activity during PKG hyperstimulation.

Epistasis appears pervasive among the pathways regulated by CDPKs. As mentioned above, activation of PKG through the application of phosphodiesterase inhibitors (e.g., zaprinast) enables parasite egress despite CDPK3 inhibition or loss (20, 60). Epistasis between PKG and CDPKs has also been observed in *Plasmodium* spp. at various stages of the intraerythrocytic cycle (18, 72, 73). Genetic interaction between PbCDPK4 (the ortholog of TgCDPK1) and PKG was revealed by a *P. berghei* screen (18). Analogously to our chemical-genetic results, PbCDPK4 becomes critical for parasite invasion and motility in a genetic background expressing a variant of PKG in which the gatekeeper residue has been mutated (PKG^{T619Q}) (18). It is inferred from phenotypes associated with PKG activity that the PKG^{T619Q} mutant is less active than wild type. As with the $TgCDPK1^{G128M}$ allele used in our chemical-genetic approach, these mutants retain sufficient kinase activity to sustain parasite viability, yet the mutation clearly places a strain on other aspects of the signaling network. Such interactions likely extend further into the network, since double knockouts of PbCDPK1 and PbCDPK4 are viable but cannot be generated in parasites expressing PKG^{T619Q} (18). The interconnectivity of CDPK networks may render them more plastic than networks with fewer connections. Indeed, studies in *P. falciparum* suggest that parasites rapidly adapt to the loss of PfCDPK1 activity, perhaps through the upregulation of other CDPKs (73, 74).

The plasticity of the signaling networks controlling egress can be manipulated through pharmacological stimuli that obscure or exaggerate the function of individual pathway components, revealing novel connectivity or dependencies. As described above, hyperactivation of the PKG pathway overcomes the inhibition of CDPK2A or CDPK3. Analogously, *P. falciparum* parasites deficient in CDPK5 fail to egress, but this

block can be overcome by hyperactivation of PKG (13, 54). The degree of pathway overstimulation, whether through ionophore or phosphodiesterase inhibitor treatment, influences the interpretation of the results—particularly since the natural levels or dynamics of these second messengers are rarely known. Hyperactivation of a pathway may also force interactions that would otherwise not occur at the basal state (75). With this context, we can consider that epistatic interactions may result from shared substrates or the redundancy of independent pathways. PKG has been shown to be a Ca^{2+} regulator in *T. gondii* and *Plasmodium* spp. (7–9, 18, 19), placing it upstream of CDPK activation. In plants, CDPKs are tuned to respond to different Ca^{2+} concentrations (43), raising the possibility that dependency on different parasite CDPKs may result from the magnitude of the Ca^{2+} surge elicited by PKG. Nevertheless, the subcellular sorting of epistatic interactions—with CDPK3 and PKG strictly localized to the PM—argues for potential overlap in their substrates as the mechanism underlying their epistasis.

Our studies also reflect some of the challenges inherent in studying protein kinases and interconnected signaling networks. While the goal is often to infer the role of a kinase in its native state, genetic perturbations may result in compensatory changes that obscure its function. While AID knockdown of CDPK1 and CDPK3 phenocopied chemical-genetic findings for egress, CDPK2A knockdown did not. Surprisingly, the discrepancy between chemical inhibition and AID depletion of CDPK2A could be attributed to the difference in CDPK1 alleles between the two systems, since partial inhibition of CDPK1 results in a stronger requirement for CDPK2A in zaprinast-stimulated egress. This is consistent with biochemical studies that revealed reduced ATP affinity of $TgCDPK1^{G128M}$ relative to the wild-type enzyme (67). Analogously, phenotypic assays such as 3D gliding motility and plaque size argue for hypomorphism of the CDPK2A-AID allele, which could only be partially relieved by tagging the kinase with an epitope (HA) rather than a fluorescent protein (mNeonGreen). Inspection of CDPK2A-AID parasites' motility suggested they may move along less-tightly wound (or lower amplitude) corkscrews compared to other strains. An altered geometry of movement may be less efficient, resulting in the smaller plaque areas observed for CDPK2A-AID parasites. Taken together, these results argue for caution in the interpretation of perturbed signaling systems, although comparison of multiple approaches can be used to infer the native function of protein kinases like CDPK2A.

Several signaling pathways converge on the regulation of microneme discharge, including those controlled by CDPK2A. Microneme discharge lies upstream of parasite egress, gliding motility, and invasion through the release of diverse proteins, including perforins that disrupt the PVM (32) and adhesins that mediate substrate attachment (76, 77). Depletion of any of the studied CDPKs decreased microneme discharge. The effect of CDPK2A depletion was observed following prolonged periods of microneme discharge (15–30 minutes). By contrast, the effect of CDPK1 and CDPK3 was already evident within 5 minutes of stimulation. This may suggest that some CDPKs regulate an initial wave of secretion, while others regulate the sustained response. Previous studies of CDPK3-knockout parasites reported normal MIC2 secretion for extracellular parasites stimulated with A23187 or ethanol (47), although intracellular parasites clearly depend on CDPK3 to permeabilize the parasitophorous vacuole upon A23187 treatment (20, 47). Differences in the sensitivity or conditions of our assays (e.g., the use of intracellular buffer in our quantitative microneme discharge assays) may have focused our assays on the responses that govern egress. Previous work also reported that the contributions of CDPK1 and CDPK3 to microneme discharge depended on the agonist used (20). Consistent with these observations and the epistatic interactions discussed above, CDPK2A may impact microneme secretion to different extents across the lytic cycle depending on the stimuli experienced by parasites.

Consistent with our observations, CDPK1 was previously implicated in parasite motility in two-dimensional (2D) analyses (20, 53). There is some ambiguity as to CDPK3's contribution to parasite motility in previous 2D analyses, depending on whether parasites were stimulated by changing from intracellular to extracellular buffer (20, 59,

70) or by treatment with A23187 (47). Nevertheless, it is clear that CDPK3-mediated phosphorylation of MyoA contributes to motility (70). Our results suggest that CDPK2A, along with CDPK1 and CDPK3, plays a critical role in gliding motility. Gliding motility seems to be sensitive to perturbations in CDPK2A, such that hypomorphism could be detected without the addition of auxin; this may result from a requirement for higher levels of kinase activity for some parasite phenotypes than others.

We demonstrated that the N-terminal extension of CDPK2A is necessary for its function. Complementing constructs that expressed a full-length version of CDPK2A mediated egress when the endogenous kinase was inhibited. The N-terminus may contain localization determinants that drive CDPK2A to the parasite periphery, although the predicted gene model lacks consensus motifs for myristoylation or palmitoylation that participate in the localization of CDPK3 to the parasite PM (20, 47). CDPK2A was also not detected in mass spectrometry data sets enriching for myristoylated (78) or palmitoylated (79) proteins. Proteomic studies have detected CDPK2A peptides spanning the coding sequence of exon 2 (exon 1 in c.1), further suggesting that the truncated c.2 sequence generated from cDNA is not the predominant species in wild-type parasites (78). Only the complementing construct driven by the endogenous 5′ UTR and promoter yielded a protein that co-localized with the endogenous CDPK2A, suggesting localization to the parasite periphery depends on endogenous regulatory signals rather than the N-terminus of the protein. We cannot exclude that an alternative translation start site is used, giving rise to dually localized species. Methionine 59 in the longer gene model may be the true start site, matching the predicted coding sequence in *Hammondia hammondi* (80). The existing data suggest that localization to the parasite periphery is not strictly required for CDPK2A's function, in contrast to CDPK3, which must be peripherally localized via myristoylation and palmitoylation to mediate parasite egress (20, 47). CDPK orthologs containing N-terminal extensions appear not to universally localize to any given compartment. PfCDPK5, which controls egress, associates with parasite membranes, possibly including the cytosolic-facing side of micronemes (13, 54), while PfCDPK3, required for ookinete motility, is cytoplasmic (14, 81). There is also precedent for signaling-related proteins to express multiple functionally distinct isoforms, often arising from alternative translational initiation. For example, in *Eimeria tenella* and *T. gondii*, one isoform of PKG is N-acylated and localizes to the PM, while the other isoform is cytoplasmic. Interestingly, either isoform can function if targeted to the PM (65, 82). Isoform diversity may further drive the plasticity of CDPK signaling networks, although this has not been formally addressed by our work.

The use of both chemical inhibition and conditional depletion to study CDPK2A function uncovered additional complexity and interconnectedness in the signaling pathways that govern the lytic cycle. We observe that CDPK1, CDPK3, and CDPK2A are all involved to varying degrees in microneme discharge, with functional consequences spanning egress, gliding motility, and invasion. We also further describe functional redundancy that structures the pathway into two signaling modules that are jointly required during parasite egress. CDPK1 and PKG play dominant roles in their respective modules, with CDPK2A and CDPK3 contributing less-essential functions. These supportive activities may be nonetheless important for parasite fitness under particular conditions. Additionally, these functional modules seem to be spatially distinct, with CDPK1/CDPK2A signaling occurring in the parasite cytoplasm, while CDPK3/PKG signaling occurs at the parasite PM (9). Understanding the topology of signaling pathways underlying key events in the parasite life cycle can help identify compensatory changes and predict phenotypic plasticity as we contemplate targeting parasite kinases for anti-parasitic therapies.

MATERIALS AND METHODS

Parasite and host cell culture

T. gondii parasites were grown in human foreskin fibroblasts (HFFs) maintained in Dulbecco's modified Eagle's medium (DMEM) (Gibco) supplemented with 3% heat-inactivated newborn calf serum (Millipore Sigma), 2 mM L-glutamine (Thermo Fisher Scientific), and 10 µg/mL gentamicin (Thermo Fisher Scientific). Where noted, DMEM supplemented with 10% heat-inactivated fetal bovine serum (FBS; Millipore Sigma), 2 mM L-glutamine (Thermo Fisher Scientific), and 10 µg/mL gentamicin was used. HFFs and *T. gondii* lines were monitored regularly and maintained as mycoplasma-free.

Strain generation

Existing *T. gondii* RH lines were used for strain construction. All strains contained Δ*ku80*/Δ*hxgprt* mutations, which facilitate homologous recombination (83). AID-tagged lines were generated using TIR1 parental parasites, which express FLAG-tagged TIR1 ubiquitin ligase (64). CDPK2A-AID-HA was generated using the high-throughput endogenous tagging system described in reference (84). Oligos were ordered from IDT. Primers, plasmids, and parasite strains used or generated in this study can be found in Table S1. Descriptions of strain generation and plasmid construction, or relevant accession numbers, are also provided in the table.

Parasite transfection

Parasites were passed through 3-µm filters, pelleted at 1,000 × *g* for 10 minutes, washed, resuspended in Cytomix (10 mM KPO_4, 120 mM KCl, 150 mM $CaCl_2$, 5 mM $MgCl_2$, 25 mM HEPES, 2 mM EDTA, 2 mM ATP, and 5 mM glutathione), and combined with DNA to a final volume of 400 µL. Electroporation used an ECM 830 Square Wave electroporator (BTX) in 4-mm cuvettes with the following settings: 1.7 kV, 2 pulses, 176 µs pulse length, and 100 ms interval.

cDNA generation

Total RNA was extracted from RH parasites using Trizol. cDNA was generated according to package instructions for SMARTer PCR cDNA synthesis kit (Clontech/Takara Bio).

Genomic DNA extraction

Extracellular parasites were pelleted at 1,000 × *g* for 10 minutes and resuspended in phosphate-buffered saline (PBS) supplemented with Proteinase K (10 µg/mL). Suspensions were incubated at 37°C for 1 hour, 50°C for 2 hours, and 95°C for 15 minutes to extract genomic DNA.

Immunoblotting

Parasite pellets were lysed in xenopus buffer (50 mM KCl, 20 mM HEPES, 2 mM $MgCl_2$, 0.1 mM EDTA pH 7.5) supplemented with 1% Triton X-100, HALT protease inhibitor cocktail (Thermo Fisher), and 10 µg/mL DNaseI (Sigma Aldrich) at room temperature for 1 hour with rotation. Lysates were combined with Laemmli buffer (for final concentration 2% SDS, 20% glycerol, 60 mM Tris HCl pH 6.8, 0.01% bromophenol blue) and 2-mercaptoethanol (1% final concentration) and boiled for 10 minutes. Samples were run on a 7.5% SDS-PAGE gel (Bio-Rad) and transferred onto a nitrocellulose membrane in transfer buffer (25 mM Tris HCl, 192 mM glycine, 0.1% SDS, 20% methanol). Blocking and all subsequent antibody incubations were performed in 5% milk in TBS-T (20 mM Tris, 138 mM NaCl, 0.1% Tween-20). Primary and secondary antibody incubations proceeded for 1 hour rocking at room temperature, with three TBS-T washes between primary and secondary and between secondary and imaging. Imaging was performed using an LI-COR Odyssey. Primary antibodies used were mouse anti-Ty (85), rabbit anti-HA

(71-5500, Invitrogen), rabbit anti-TgACT1 (86), mouse anti-HA (16B12, BioLegend), and guinea pig anti-CDPK1 (87). Secondary antibodies were anti-mouse-800CW (LI-COR), anti-rabbit-680RD (LI-COR), or anti-guinea pig-680RD (LI-COR).

Live cell imaging

Parasites were inoculated onto glass-bottom 35-mm dishes (Mattek) containing HFFs. At 24 hours post-infection, intracellular parasites were imaged with an Eclipse Ti microscope (Nikon Instruments, Melville, NY) with a 60× objective using the NIS Elements imaging software and a Zyla 4.2 sCMOS camera. FIJI software was used for image processing.

Immunofluorescence assays

Parasites were inoculated onto coverslips containing HFFs. At 24 hours post-infection, intracellular parasites were fixed with 4% formaldehyde and permeabilized with 0.05% saponin in PBS. Nuclei were stained with Hoechst 33258 (Santa Cruz), and coverslips were mounted in Prolong Diamond (Thermo Fisher Scientific). Ty was detected using a mouse monoclonal antibody (85). HA was detected using a rabbit monoclonal antibody (71-5500, Invitrogen). Primary antibodies were detected with anti-mouse Alexa Fluor 488 and anti-rabbit Alexa Fluor 594 secondary antibodies (Invitrogen). Images were acquired with an Eclipse Ti microscope (Nikon Instruments) with a 60× objective using the NIS Elements imaging software and a Zyla 4.2 sCMOS camera. FIJI software was used for image processing.

Egress assays

Egress was quantified in a plate-based manner as in reference 62. HFF monolayers in a clear bottomed 96-well plate were infected with parasites and allowed to incubate for 24 hours before exchanging media for FluoroBrite DMEM (Thermo Fisher Scientific) supplemented with 10% FBS and applying pre-treatments according to experiment type. Three images were taken before zaprinast (final concentration 500 µM; MilliPore Sigma) or A23187 (final concentration 8 µM; MilliPore Sigma), and 4′,6-diamidino-2-phenylindole (DAPI) (final concentration 5 ng/mL) was added; imaging of DAPI-stained host cell nuclei (HCN) continued for 9 additional minutes before 1% Triton X-100 was added to all wells to determine the total number of HCN. Imaging was performed at 37°C and 5% CO_2 using a BioTek Cytation 3 imaging multimode reader with a 4× objective. Percent egress was calculated as [(nuclei at $time_n$ − nuclei at $time_1$)/(nuclei at $time_{final}$ − nuclei at $time_1$)] * 100, and egress efficiency was normalized to egress of vehicle-treated parasites (percentage of vehicle). Multiplicity of infection was determined by performing immunofluorescence on a parallel plate of parasite-infected HFFs. Briefly, infected monolayers were fixed and permeabilized with 100% methanol for 2 minutes. Parasites were stained with either rabbit anti-TgALD (88) or guinea pig anti-CDPK1 antibody (87) and anti-rabbit or anti-guinea pig Alexa Fluor 594 secondary antibody, and nuclei were stained with Hoechst 33258 (Santa Cruz Biotechnology). Imaging was performed using a BioTek Cytation 3 imaging multimode reader with a 20× objective, and parasite vacuoles and host nuclei were manually counted. For analog-sensitive (AS) kinase egress assays, HFFs were infected with 5×10^4 parasites per well and treated with 3 µM 3-MB-PP1 (MilliPore Sigma) or equivalent dilution of dimethyl sulfoxide (DMSO) for 20 minutes prior to analysis. For AID egress assays, HFFs were infected with 1×10^5 parasites per well of TIR1 parental or CDPK-AID lines and treated with 500 µM IAA or equivalent dilution of PBS for 3 hours prior to analysis. For endpoint assays, HFFs were infected with 1×10^5 parasites per well of TIR1 parental or CDPK-AID lines. Pre-treatment consisted of 500 µM IAA or equivalent dilution of PBS for 3 hours, followed by 3-MB-PP1 (series from 2.5 µM to 0.039 µM) or equivalent dilution of DMSO for 30 minutes prior to analysis, and wells were stimulated to egress with zaprinast (final concentration 500 µM) for 20 minutes; all incubations were performed at 37°C and 5% CO_2. Images were collected pre-stimulation ($time_{pre}$), 10 minute post-addition of zaprinast and DAPI ($time_{stim}$), and 1 minute

post-addition of 1% Triton X-100 ($time_{final}$). Percent egress was calculated as [(nuclei at $time_{stim}$ − nuclei at $time_{pre}$)/(nuclei at $time_{final}$ − nuclei at $time_{pre}$)] * 100 and normalized to wells that did not receive IAA or 3-MB-PP1 for each strain. EC_{50} was determined by non-linear regression analysis performed using the non-sigmoidal dose-response with variable slope function in GraphPad Prism, with top constrained to 100 and bottom constrained to 0; significance was calculated using an F-test to determine if all data (±IAA) fit a single curve.

For lactate dehydrogenase (LDH) release assays, HFFs were infected with 5×10^4 parasites per well and treated with 3-MB-PP1 at concentrations ranging from 5 µM to 0.01 nM or equivalent dilution of DMSO for 20 minutes prior to analysis. Parasites were stimulated with A23187 (final concentration 1 µM; MilliPore Sigma), and egress was allowed to proceed for 5 minutes at 37°C before supernatants were collected by centrifugation. Samples were prepared according to Cytotox 96 Non-Radioactive Cytotoxicity Assay (Promega) instructions, and absorbance at 490 nm was measured. Percent egress was calculated as (sample − uninfected well)/(lysis control − uninfected well) * 100 and normalized to wells that did not receive 3-MB-PP1 for each strain. EC_{50} was determined by non-linear regression analysis performed using the non-sigmoidal dose-response with variable slope function in GraphPad Prism; significance was calculated by unpaired *t*-test.

Invasion assays

Briefly, parasite vacuoles were mechanically dissociated and filtered through 5-µm filters, pelleted, and resuspended in invasion media (HEPES-buffered DMEM without phenol red) supplemented with 1% FBS. HFF monolayers in clear-bottom 96-well plates were incubated with parasite suspensions for 10 minutes at 37°C to stimulate invasion after centrifuging the plates at 290 × *g* and room temperature for 5 minutes. Wells were fixed with 4% formaldehyde and followed by antibody staining to differentiate between extracellular and total parasites and to detect nuclei. Samples were imaged using a BioTek Cytation 3 imaging multimode reader with a 20× objective and imaging in montage mode.

For AS kinase invasion assays, parasites were pre-treated with 3-MB-PP1 (0.33 µM final concentration) or an equivalent dilution of DMSO in invasion media for 20 minutes at 37°C, then 1×10^5 parasites were added to 3 wells of a clear-bottom 96-well plate containing HFFs. Following incubation and fixation, extracellular parasites were stained with mouse anti-SAG1 antibody (89) conjugated to Alexa Fluor 594. All parasites were detected by permeabilizing with 0.25% Triton X-100 and staining with anti-SAG1 antibody conjugated to Alexa Fluor 488, and nuclei were stained with DAPI. The number of invaded parasites per field of view was counted using a size-based macro and normalized to the number of host cells in the same field of view (intracellular Tg/HCN). The final invasion efficiency for each replicate was normalized to the invaded parasites per HCN of the DMSO-treated parasites (percentage of vehicle).

For AID invasion assays, parasite lines were each passed to two flasks of HFFs. Twenty-four hours pre-analysis, one flask was supplemented with vehicle (PBS) and the second flask was supplemented with IAA to a final concentration of 500 µM. Following parasite harvest, 2×10^5 parasites were added to 3 wells of a clear-bottom 96-well plate containing HFFs. Following incubation and fixation, extracellular parasites were stained with mouse anti-SAG1 antibody (89). All parasites were detected by permeabilizing with 0.25% Triton X-100 and staining with rabbit anti-GAP45, generated as previously described (90) and kindly provided by R. D. Ethridge (University of Georgia, Athens). Cells were subsequently stained with anti-rabbit Alexa Fluor 594 antibody (Invitrogen), anti-mouse Alexa Fluor 488 antibody (Invitrogen), and Hoechst 33258 (Santa Cruz Biotechnology). Images were analyzed using custom FIJI macros to count the number of parasites and HCN (55), plotted as intracellular Tg/HCN.

Plaque assays

CDPK-AID and TIR1 parental parasites were inoculated into 6-well plates or 15-cm dishes of HFFs maintained in DMEM supplemented with 10% FBS and incubated overnight before supplementing with IAA to a final concentration of 500 µM or with PBS. Where indicated, plates were also supplemented with 3-MB-PP1 to a final concentration of 40 nM or with DMSO. Plates were allowed to grow undisturbed for 8 days then washed with PBS, and fixed for 10 minutes at room temperature with 100% ethanol. Staining was performed for 5 minutes at room temperature with crystal violet solution, followed by two washes with PBS, one wash with water, and drying overnight. Plaques were counted manually, and plaque areas were measured using FIJI software.

FACS analysis

For IAA-induced depletion experiments, intracellular parasites were treated with either 500 µM IAA or an equivalent dilution of PBS for 1, 3, or 24 hours. Following treatment, parasites were mechanically dissociated by passing through a 27-gauge needle, isolated by filtration, and analyzed by flow cytometry with a Miltenyi MACSQuant VYB; plots were prepared using FlowJo software.

Competition assays

Freshly lysed CDPK2A-AID, CDPK2A-AID-HA, or CDPK3-AID parasites were combined in equal proportions with TIR1/IMC1-TdTom (84) and analyzed by flow cytometry with a Miltenyi MACSQuant VYB to determine proportions of initial mixtures. Mixtures were used to inoculate a monolayer of HFFs, and after each subsequent lysis of the monolayer, the pools were passaged onto fresh monolayers with media containing 500 µM IAA or an equivalent dilution of PBS. Pools were analyzed by flow cytometry at each lysis. Gates were drawn using FlowJo software, and the percentage of CDPK-AID parasites was plotted for each passage.

Microneme protein secretion assays

CDPK-*Gaussia* luciferase (GLuc) lines were each used to inoculate two flasks of HFFs. Twenty-four hours pre-analysis, one flask was supplemented with vehicle (PBS) and the second flask was supplemented with IAA to a final concentration of 500 µM. Parasite vacuoles were mechanically disrupted, and parasites were filtered through 5-µm filters, pelleted, and resuspended in cold intracellular buffer (ICB) with free Ca^{2+} clamped at 100 nM (ICB: 137 mM KCl, 5 mM NaCl, 20 mM HEPES, 10 mM $MgCl_2$). 1×10^6 parasites were combined with ICB or ICB supplemented with 3% FBS and zaprinast (500 µM) into 3 wells of 96-well round-bottom plate and incubated for 5 or 30 minutes at 37°C and 5% CO_2 to stimulate secretion. Excreted/secreted antigen (ESA)–containing supernatants were collected by centrifugation at 1,200 × *g* for 8 minutes at 4°C to pellet parasites. Parasite lysates were prepared according to Pierce Gaussia Luciferase Glow Assay Kit (Thermo Fisher Scientific) and plated in triplicate with wells containing lysate from 6.6×10^5, 2.2×10^5, and 7.4×10^4 parasite-equivalents for each strain with or without IAA. ESAs and lysates were plated in white-bottom assay plates (PerkinElmer No. 6002290) and incubated at room temperature for 5 minutes with substrate-containing assay solution before detecting luciferase signal using a BioTek Cytation 3 multimode reader. For each independent replicate, background luminescence (from wells without parasites) was subtracted from ESA luciferase values.

For immunoblot assays, CDPK1-AID and CDPK2A-AID lines were each used to inoculate two flasks of HFFs. Twenty-four hours pre-analysis, one flask was supplemented with vehicle (PBS) and the second flask was supplemented with IAA to a final concentration of 500 µM. Freshly egressed parasites were filtered through 5-µm filters, pelleted, and resuspended in cold DMEM (without serum supplementation) to a concentration of 6×10^8 parasites/mL. 3×10^7 parasites were combined with DMEM or DMEM

supplemented with 3% FBS and 1% ethanol and incubated for 15 minutes at 37°C to stimulate secretion. Excreted/secreted antigen (ESA)-containing supernatants were collected by centrifugation at 1,200 × *g* for 8 minutes at 4°C to pellet parasites. Parasite lysates were prepared by combining 3×10^7 parasites in 50 µL with an equal volume of DMEM, and both lysates and ESAs were combined with Laemmli buffer (for final concentration 2% SDS, 20% glycerol, 60 mM Tris HCl pH 6.8, 0.01% bromophenol blue) and 2-mercaptoethanol (1% final concentration). ESA and lysate samples were boiled for 10 minutes prior to migrating on 4%–15% SDS-PAGE gel (Bio-Rad), and immunoblotting and imaging proceeded as above. Primary antibodies used were mouse anti-MIC2 (6D10) (27) and rabbit anti-ALD1 (88). Secondary antibodies were anti-mouse-800CW (LI-COR) and anti-rabbit-680RD (LI-COR).

Three-dimensional (3D) motility

Parasites in HFF cells were treated with either 500 µM auxin or PBS for 3 hours prior to harvest by mechanical dissociation. Pitta imaging chambers containing Hoechst 33342-stained parasites embedded in polymerized Matrigel were prepared as previously described (69). A Nikon Eclipse TE300 epifluorescence microscope (Nikon Instruments) equipped with a 20× (0.65 pixel/µm) PlanApo λ (NA 0.75) objective and NanoScanZ piezo Z stage insert (Prior Scientific, Rockland, MA) was used to image the fluorescently labeled parasite nuclei. Time-lapse video stacks were collected with an iXON Life 888 EMCCD camera (Andor Technology, Belfast, Ireland) using NIS Elements software v.5.11 (Nikon Instruments) and pE-4000 LED illumination (CoolLED, Andover, England). Images (1,024 pixel × 384 pixel) were collected 1 µm apart in *z*, spanning 40 µm. Each *z* slice was imaged once (HA-expressing parasites) or twice (mNeonGreen-expressing parasites), at excitation wavelengths 385 nm (Hoechst) and 490 nm (mNeonGreen parasites only), each for 15 ms, before moving to the next *z* slice. The same volume was successively imaged 120 or 60 times, respectively, over the course of 79 seconds. The volume of each video stack was, therefore, 665.6 µm × 249.6 µm × 40 µm (*x*, *y*, *z*), and each data set contained 1 × 120 or 2 × 60 stacks. The camera was set to trigger mode, no binning, readout speed of 30 MHz, conversion gain of 3.8×, and EM gain setting of 300. For CDPK2A-AID-HA comparisons, imaging did not include the 490-nm wavelength.

Data sets were analyzed in Imaris ×64 v. 9.2.0 (Bitplane AG, Zurich, Switzerland). Parasites were tracked using the ImarisTrack module within a 1,018 × 380-pixel region of interest to prevent artifacts from tracking objects near the border. Spot detection was used to estimate spot diameters of 4.0 × 4.0 × 8.0 µm (*x*, *y*, *z*) for the fluorescently labeled nuclei. A maximum distance of 6.0 µm and a maximum gap size of 2 were applied to the tracking algorithm. Tracks with durations under 10 seconds or displacements of less than 2 µm were discarded to avoid tracking artifacts and parasites moving by Brownian motion, respectively (69). Accurate tracking was confirmed by visual inspection of parasite movements superimposed on their calculated trajectories. The mNeonGreen signal was used to confirm the depletion of the mNeonGreen-Ty-AID-tagged CDPK protein in tracked parasites; auxin-treated parasites that remained positive for mNeonGreen were excluded from the analysis.

ACKNOWLEDGMENTS

We thank L. D. Sibley (Washington University in St. Louis) for the TIR1 strain, aldolase antibody, and MIC2 6D10 hybridoma; S. M. Sidik for the generation of the Cas9 nickase plasmid; B. M. Markus for the generation of the mNeonGreen-AID-Ty plasmid; R. D. Etheridge (University of Georgia, Athens) for the GAP45 antibody; VEuPathDB; and all contributors to this resource.

This work was supported by grants from the National Institutes of Health to S.L. (R01AI144369) and G.E.W. (R01AI139201) and training grant and fellowship support for R.V.S. (T32AI055402 and F31AI145214).

E.S. and S.L. designed the overall study and experiments. C.G.H. generated and validated the AS kinase strains and performed initial construction of complementing

constructs. R.V.S. and R.S.K. performed and quantified the gliding motility experiments. A.L.H. generated the CDPK2A-AID-HA strain. E.S. performed all remaining parasite strain construction and experiments. E.S. and S.L. wrote the manuscript, and all authors reviewed, offered input, and approved the final draft.

AUTHOR AFFILIATIONS

[1]Whitehead Institute, Cambridge, Massachusetts, USA
[2]Department of Microbiology and Molecular Genetics, University of Vermont Larner College of Medicine, Burlington, Vermont, USA
[3]Biology Department, MIT, Cambridge, Massachusetts, USA

PRESENT ADDRESS

Caroline G. Hackett, Regeneron Pharmaceuticals, Tarrytown, New York, USA

AUTHOR ORCIDs

Emily Shortt http://orcid.org/0009-0009-7625-4772
Caroline G. Hackett http://orcid.org/0009-0004-9491-3018
Robyn S. Kent http://orcid.org/0000-0002-2584-4694
Gary E. Ward http://orcid.org/0000-0003-4138-3055
Sebastian Lourido http://orcid.org/0000-0002-5237-1095

FUNDING

Funder	Grant(s)	Author(s)
HHS | National Institutes of Health (NIH)	R01AI144369	Sebastian Lourido
HHS | National Institutes of Health (NIH)	R01AI139201	Gary E WARD
HHS | National Institutes of Health (NIH)	T32AI055402	Rachel V Stadler
HHS | National Institutes of Health (NIH)	F31AI145214	Rachel V Stadler

AUTHOR CONTRIBUTIONS

Emily Shortt, Conceptualization, Data curation, Investigation, Visualization, Writing – original draft, Writing – review and editing, Funding acquisition | Caroline G. Hackett, Investigation | Rachel V. Stadler, Data curation, Investigation, Writing – review and editing | Robyn S. Kent, Investigation, Writing – review and editing | Alice L. Herneisen, Resources | Gary E. Ward, Conceptualization, Writing – review and editing, Funding acquisition | Sebastian Lourido, Conceptualization, Writing – review and editing, Funding acquisition, Supervision

DATA AVAILABILITY

Primers, plasmids, and parasite strains used or generated in this study can be found in Table S1. Oligos, plasmids, and strains generated within this study are available from the corresponding author by request.

ADDITIONAL FILES

The following material is available online.

Supplemental Material

Supplemental Figures (mBio01358-23-S0001.pdf). Figures S1-S6.
Table S1 (mBio01358-23-S0002.xlsx). Primers, plasmids, and parasite strains used or generated in this study.

REFERENCES

1. Clapham DE. 2007. Calcium signaling. Cell 131:1047–1058. https://doi.org/10.1016/j.cell.2007.11.028
2. Endo T, Sethi KK, Piekarski G. 1982. *Toxoplasma gondii*: calcium Ionophore A23187-mediated exit of trophozoites from infected murine macrophages. Exp Parasitol 53:179–188. https://doi.org/10.1016/0014-4894(82)90059-5
3. Moreno SNJ, Zhong L. 1996. Acidocalcisomes in *Toxoplasma gondii* tachyzoites. Biochem Jhttps://doi.org/10.1042/bj3130655.
4. Stommel EW, Ely KH, Schwartzman JD, Kasper LH. 1997. *Toxoplasma gondii*: dithiol-induced Ca2+ flux causes egress of parasites from the parasitophorous vacuole. Exp Parasitol 87:88–97. https://doi.org/10.1006/expr.1997.4187
5. Borges-Pereira L, Budu A, McKnight CA, Moore CA, Vella SA, Hortua Triana MA, Liu J, Garcia CRS, Pace DA, Moreno SNJ. 2015. Calcium signaling throughout the *Toxoplasma gondii* lytic cycle. J Biol Chem290:26914–26926. https://doi.org/10.1074/jbc.M115.652511
6. Howard BL, Harvey KL, Stewart RJ, Azevedo MF, Crabb BS, Jennings IG, Sanders PR, Manallack DT, Thompson PE, Tonkin CJ, Gilson PR. 2015. Identification of potent phosphodiesterase inhibitors that demonstrate cyclic nucleotide-dependent functions in apicomplexan parasites. ACS Chem Biol 10:1145–1154. https://doi.org/10.1021/cb501004q
7. Sidik SM, Hortua Triana MA, Paul AS, El Bakkouri M, Hackett CG, Tran F, Westwood NJ, Hui R, Zuercher WJ, Duraisingh MT, Moreno SNJ, Lourido S. 2016. Using a genetically encoded sensor to identify inhibitors of *Toxoplasma gondii* Ca2+ signaling. J Biol Chem 291:9566–9580. https://doi.org/10.1074/jbc.M115.703546
8. Brown KM, Lourido S, Sibley LD. 2016. Serum albumin stimulates protein kinase G-dependent microneme secretion in *Toxoplasma gondii*. J Biol Chem 291:9554–9565. https://doi.org/10.1074/jbc.M115.700518
9. Nofal SD, Dominicus C, Broncel M, Katris NJ, Flynn HR, Arrizabalaga G, Botté CY, Invergo BM, Treeck M. 2022. A positive feedback loop mediates crosstalk between calcium, cyclic nucleotide and lipid signalling in calcium-induced *Toxoplasma gondii egress*. PLoS Pathog 18:e1010901. https://doi.org/10.1371/journal.ppat.1010901
10. Lovett JL, Sibley LD. 2003. Intracellular calcium stores in *Toxoplasma gondii* govern invasion of host cells. J Cell Sci 116:3009–3016. https://doi.org/10.1242/jcs.00596
11. Singh S, Alam MM, Pal-Bhowmick I, Brzostowski JA, Chitnis CE, Blackman MJ. 2010. Distinct external signals trigger sequential release of apical organelles during erythrocyte invasion by malaria parasites. PLoS Pathog 6:e1000746. https://doi.org/10.1371/journal.ppat.1000746
12. Agarwal S, Singh MK, Garg S, Chitnis CE, Singh S. 2013. Ca(2+) -mediated exocytosis of subtilisin-like protease 1: a key step in egress of *Plasmodium falciparum* merozoites. Cell Microbiol 15:910–921. https://doi.org/10.1111/cmi.12086
13. Dvorin JD, Martyn DC, Patel SD, Grimley JS, Collins CR, Hopp CS, Bright AT, Westenberger S, Winzeler E, Blackman MJ, Baker DA, Wandless TJ, Duraisingh MT. 2010. A plant-like kinase in *Plasmodium falciparum* regulates parasite egress from erythrocytes. Science 328:910–912. https://doi.org/10.1126/science.1188191
14. Siden-Kiamos I, Ecker A, Nybäck S, Louis C, Sinden RE, Billker O. 2006. *Plasmodium berghei* calcium-dependent protein kinase 3 is required for ookinete gliding motility and mosquito midgut invasion. Mol Microbiol 60:1355–1363. https://doi.org/10.1111/j.1365-2958.2006.05189.x
15. Wetzel DM, Chen LA, Ruiz FA, Moreno SNJ, Sibley LD. 2004. Calcium-mediated protein secretion potentiates motility in *Toxoplasma gondii*. J Cell Sci 117:5739–5748. https://doi.org/10.1242/jcs.01495
16. Pace DA, McKnight CA, Liu J, Jimenez V, Moreno SNJ. 2014. Calcium entry in *Toxoplasma gondii* and its enhancing effect of invasion-linked traits. J Biol Chem 289:19637–19647. https://doi.org/10.1074/jbc.M114.565390
17. Lourido S, Moreno SNJ. 2015. The calcium signaling toolkit of the apicomplexan parasites *Toxoplasma gondii* and *Plasmodium* spp. Cell Calcium 57:186–193. https://doi.org/10.1016/j.ceca.2014.12.010
18. Fang H, Gomes AR, Klages N, Pino P, Maco B, Walker EM, Zenonos ZA, Angrisano F, Baum J, Doerig C, Baker DA, Billker O, Brochet M. 2018. Epistasis studies reveal redundancy among calcium-dependent protein kinases in motility and invasion of malaria parasites. Nat Commun 9:4248. https://doi.org/10.1038/s41467-018-06733-w
19. Brochet M, Collins MO, Smith TK, Thompson E, Sebastian S, Volkmann K, Schwach F, Chappell L, Gomes AR, Berriman M, Rayner JC, Baker DA, Choudhary J, Billker O. 2014. Phosphoinositide metabolism links cGMP-dependent protein kinase G to essential Ca^{2+} signals at key decision points in the life cycle of malaria parasites2+ Phosphoinositide metabolism links cGMP-dependent protein kinase G to essential Ca^{2+} signals at key decision points in the life cycle of malaria parasites. PLoS Biol 12:e1001806. https://doi.org/10.1371/journal.pbio.1001806
20. Lourido S, Tang K, Sibley LD. 2012. Distinct signalling pathways control *Toxoplasma* egress and host-cell invasion. EMBO J 31:4524–4534. https://doi.org/10.1038/emboj.2012.299
21. Collins CR, Hackett F, Strath M, Penzo M, Withers-Martinez C, Baker DA, Blackman MJ. 2013. Malaria parasite cGMP-dependent protein kinase regulates blood stage merozoite secretory organelle discharge and egress. PLoS Pathog 9:e1003344. https://doi.org/10.1371/journal.ppat.1003344
22. Howard BL, Harvey KL, Stewart RJ, Azevedo MF, Crabb BS, Jennings IG, Sanders PR, Manallack DT, Thompson PE, Tonkin CJ, Gilson PR. 2015. Identification of potent phosphodiesterase inhibitors that demonstrate cyclic nucleotide-dependent functions in apicomplexan parasites. ACS Chem Biol 10:1145–1154.
23. Bullen HE, Jia Y, Yamaryo-Botté Y, Bisio H, Zhang O, Jemelin NK, Marq J-B, Carruthers V, Botté CY, Soldati-Favre D. 2016. Phosphatidic acid-mediated signaling regulates microneme secretion in *Toxoplasma*. Cell Host Microbe 19:349–360. https://doi.org/10.1016/j.chom.2016.02.006
24. Carruthers VB, Giddings OK, Sibley LD. 1999. Secretion of micronemal proteins is associated with *Toxoplasma* invasion of host cells. Cell Microbiol 1:225–235. https://doi.org/10.1046/j.1462-5822.1999.00023.x
25. Carruthers VB, Sibley LD. 1999. Mobilization of intracellular calcium stimulates microneme discharge in *Toxoplasma gondii*. Mol Microbiol 31:421–428. https://doi.org/10.1046/j.1365-2958.1999.01174.x
26. Carruthers Vern B., Moreno SNJ, Sibley DL. 1999. Ethanol and acetaldehyde elevate intracellular [Ca2+] and stimulate microneme discharge in *Toxoplasma gondii*. Biochem J 342:379–386. https://doi.org/10.1042/bj3420379
27. Carruthers V.B, Sherman GD, Sibley LD. 2000. The *Toxoplasma* adhesive protein Mic2 is proteolytically processed at multiple sites by two parasite-derived proteases. J Biol Chem 275:14346–14353. https://doi.org/10.1074/jbc.275.19.14346
28. Jacot D, Tosetti N, Pires I, Stock J, Graindorge A, Hung Y-F, Han H, Tewari R, Kursula I, Soldati-Favre D. 2016. An apicomplexan actin-binding protein serves as a connector and lipid sensor to coordinate motility and invasion. Cell Host Microbe 20:731–743. https://doi.org/10.1016/j.chom.2016.10.020
29. Sultan AA, Thathy V, Frevert U, Robson KJ, Crisanti A, Nussenzweig V, Nussenzweig RS, Ménard R. 1997. TRAP is necessary for gliding motility and infectivity of *Plasmodium* sporozoites. Cell 90:511–522. https://doi.org/10.1016/s0092-8674(00)80511-5
30. Lagal V, Binder EM, Huynh M-H, Kafsack BFC, Harris PK, Diez R, Chen D, Cole RN, Carruthers VB, Kim K. 2010. *Toxoplasma gondii* protease TgSUB1 is required for cell surface processing of micronemal adhesive complexes and efficient adhesion of tachyzoites. Cell Microbiol 12:1792–1808. https://doi.org/10.1111/j.1462-5822.2010.01509.x
31. Dowse T, Soldati D. 2004. Host cell invasion by the apicomplexans: the significance of microneme protein proteolysis. Curr Opin Microbiol 7:388–396. https://doi.org/10.1016/j.mib.2004.06.013
32. Kafsack BFC, Pena JDO, Coppens I, Ravindran S, Boothroyd JC, Carruthers VB. 2009. Rapid membrane disruption by a perforin-like protein facilitates parasite exit from host cells. Science 323:530–533. https://doi.org/10.1126/science.1165740
33. Roiko MS, Carruthers VB. 2013. Functional dissection of *Toxoplasma gondii* perforin-like protein 1 reveals a dual domain mode of membrane binding for cytolysis and parasite egress. J Biol Chem 288:8712–8725. https://doi.org/10.1074/jbc.M113.450932
34. Sivagurunathan S, Heaslip A, Liu J, Hu K. 2013. Identification of functional modules of AKMT, a novel lysine methyltransferase regulating the motility of *Toxoplasma gondii*. Mol Biochem Parasitol 189:43–53. https://doi.org/10.1016/j.molbiopara.2013.05.004

35. Deligianni E, Morgan RN, Bertuccini L, Wirth CC, Silmon de Monerri NC, Spanos L, Blackman MJ, Louis C, Pradel G, Siden-Kiamos I. 2013. A perforin-like protein mediates disruption of the erythrocyte membrane during egress of *Plasmodium berghei* male gametocytes. Cell Microbiol 15:1438–1455. https://doi.org/10.1111/cmi.12131
36. Wirth CC, Glushakova S, Scheuermayer M, Repnik U, Garg S, Schaack D, Kachman MM, Weißbach T, Zimmerberg J, Dandekar T, Griffiths G, Chitnis CE, Singh S, Fischer R, Pradel G. 2014. Perforin - like protein PPLP 2 permeabilizes the red blood cell membrane during egress of *Plasmodium falciparum* gametocytes. Cell Microbiol 16:709–733. https://doi.org/10.1111/cmi.12288
37. Garg S, Agarwal S, Kumar S, Yazdani SS, Chitnis CE, Singh S. 2013. Calcium-dependent permeabilization of erythrocytes by a perforin-like protein during egress of malaria parasites. Nat Commun 4:1736. https://doi.org/10.1038/ncomms2725
38. Chen XM, O'Hara SP, Huang BQ, Nelson JB, Lin JJC, Zhu G, Ward HD, LaRusso NF. 2004. Apical organelle discharge by *Cryptosporidium parvum* is temperature, cytoskeleton, and intracellular calcium dependent and required for host cell invasion. Infect Immun 72:6806–6816. https://doi.org/10.1128/IAI.72.12.6806-6816.2004
39. Wiersma HI, Galuska SE, Tomley FM, Sibley LD, Liberator PA, Donald RGK. 2004. A role for coccidian cGMP-dependent protein kinase in motility and invasion. Int J Parasitol 34:369–380. https://doi.org/10.1016/j.ijpara.2003.11.019
40. Gantt S, Persson C, Rose K, Birkett AJ, Abagyan R, Nussenzweig V. 2000. Antibodies against thrombospondin-related anonymous protein do not inhibit *Plasmodium sporozoite* infectivity *in vivo*. Infect Immun 68:3667–3673. https://doi.org/10.1128/IAI.68.6.3667-3673.2000
41. Herneisen AL, Li Z-H, Chan AW, Moreno SNJ, Lourido S. 2022. Temporal and thermal profiling of the *Toxoplasma proteome* implicates parasite protein phosphatase 1 in the regulation of Ca2+-responsive pathways. Elife 11:e80336. https://doi.org/10.7554/eLife.80336
42. Billker O, Lourido S, Sibley LD. 2009. Calcium-dependent signaling and kinases in apicomplexan parasites. Cell Host Microbe 5:612–622.
43. Harper JF, Breton G, Harmon A. 2004. Decoding Ca(2+) signals through plant protein Kinases. Annu Rev Plant Biol 55:263–288. https://doi.org/10.1146/annurev.arplant.55.031903.141627
44. Yip Delormel T, Boudsocq M. 2019. Properties and functions of calcium-dependent protein kinases and their relatives in *Arabidopsis thaliana*. New Phytol 224:585–604. https://doi.org/10.1111/nph.16088
45. Harmon AC, Gribskov M, Harper JF. 2000. CDPKs - a kinase for every Ca2+ signal? Trends Plant Sci 5:154–159.
46. Lee JY, Yoo BC, Harmon AC. 1998. Kinetic and calcium-binding properties of three calcium-dependent protein kinase isoenzymes from soybean. Biochemistry 37:6801–6809. https://doi.org/10.1021/bi980062q
47. McCoy JM, Whitehead L, van Dooren GG, Tonkin CJ. 2012. TgCDPK3 regulates calcium-dependent egress of *Toxoplasma gondii* from host cells. PLoS Pathog 8:e1003066. https://doi.org/10.1371/journal.ppat.1003066
48. Long S, Wang Q, Sibley LD. 2016. Analysis of noncanonical calcium-dependent protein kinases in *Toxoplasma gondii* by targeted gene deletion using CRISPR/Cas9. Infect Immun 84:1262–1273. https://doi.org/10.1128/IAI.01173-15
49. Morlon-Guyot J, Berry L, Chen C-T, Gubbels M-J, Lebrun M, Daher W. 2014. The *Toxoplasma gondii* calcium-dependent protein kinase 7 is involved in early steps of parasite division and is crucial for parasite survival. Cell Microbiol 16:95–114. https://doi.org/10.1111/cmi.12186
50. Bansal P, Antil N, Kumar M, Yamaryo-Botté Y, Rawat RS, Pinto S, Datta KK, Katris NJ, Botté CY, Prasad TSK, Sharma P. 2021. Protein kinase TgCDPK7 regulates vesicular trafficking and phospholipid synthesis in *Toxoplasma gondii*. PLoS Pathog 17:e1009325. https://doi.org/10.1371/journal.ppat.1009325
51. Billker O, Dechamps S, Tewari R, Wenig G, Franke-Fayard B, Brinkmann V. 2004. Calcium and a calcium-dependent protein kinase regulate gamete formation and mosquito transmission in a malaria parasite. Cell 117:503–514.
52. Bansal A, Molina-Cruz A, Brzostowski J, Mu J, Miller LH, Sibley LD. 2017. *Plasmodium falciparum* calcium-dependent protein kinase 2 is critical for male gametocyte exflagellation but not essential for asexual proliferation . mBio 8. https://doi.org/10.1128/mBio.01656-17
53. Lourido S, Shuman J, Zhang C, Shokat KM, Hui R, Sibley LD. 2010. Calcium-dependent protein kinase 1 is an essential regulator of exocytosis in *Toxoplasma*. Nature 465:359–362. https://doi.org/10.1038/nature09022
54. Absalon S, Blomqvist K, Rudlaff RM, DeLano TJ, Pollastri MP, Dvorin JD, Miller LH. 2018. Calcium-dependent protein kinase 5 is required for release of egress-specific organelles in *Plasmodium falciparum* . mBio 9. https://doi.org/10.1128/mBio.00130-18
55. Sidik SM, Huet D, Ganesan SM, Huynh M-H, Wang T, Nasamu AS, Thiru P, Saeij JPJ, Carruthers VB, Niles JC, Lourido S. 2016. A genome-wide CRISPR screen in *Toxoplasma* identifies essential apicomplexan genes. Cell 166:1423–1435. https://doi.org/10.1016/j.cell.2016.08.019
56. Wernimont AK, Artz JD, Finerty P, Lin Y-H, Amani M, Allali-Hassani A, Senisterra G, Vedadi M, Tempel W, Mackenzie F, Chau I, Lourido S, Sibley LD, Hui R. 2010. Structures of apicomplexan calcium-dependent protein kinases reveal mechanism of activation by calcium. Nat Struct Mol Biol 17:596–601. https://doi.org/10.1038/nsmb.1795
57. Sugi T, Kato K, Kobayashi K, Watanabe S, Kurokawa H, Gong H, Pandey K, Takemae H, Akashi H. 2010. Use of the kinase inhibitor analog 1NmM-PP1 reveals a role for *Toxoplasma gondii* CDPK1 in the invasion step. Eukaryot Cell 9:667–670. https://doi.org/10.1128/EC.00351-09
58. Bishop AC, Shah K, Liu Y, Witucki L, Kung C, Shokat KM. 1998. Design of allele-specific inhibitors to probe protein kinase signaling. Curr Biol 8:257–266. https://doi.org/10.1016/s0960-9822(98)70198-8
59. Garrison E, Treeck M, Ehret E, Butz H, Garbuz T, Oswald BP, Settles M, Boothroyd J, Arrizabalaga G. 2012. A forward genetic screen reveals that calcium-dependent protein kinase 3 regulates egress in *Toxoplasma*. PLoS Pathog 8:e1003049. https://doi.org/10.1371/journal.ppat.1003049
60. Stewart RJ, Whitehead L, Nijagal B, Sleebs BE, Lessene G, McConville MJ, Rogers KL, Tonkin CJ. 2017. Analysis of Ca2+ mediated signaling regulating *Toxoplasma* infectivity reveals complex relationships between key molecules. Cell Microbiol 19. https://doi.org/10.1111/cmi.12685
61. Riss T, Niles A, Moravec R, Karassina N, Vidugiriene J, In Markossian, S, Grossman, A, Brimacombe, K, Arkin, M, Auld, D, Austin, C, Baell, J, Chung, TDY, Coussens, NP, Dahlin, JL, Devanarayan, V, Foley, TL, Glicksman, M, Gorshkov, K, Haas, JV, Hall, MD, Hoare, S, Inglese, J, Iversen, PW, Kales, SC, Lal-Nag, M, Li, Z, McGee, J, McManus, O, Riss, T, Saradjian, P, Sittampalam, GS, Tarselli, M, Trask, OJ, Jr, Wang, Y, Weidner, JR, Wildey, MJ, Wilson, K, Xia, M, Xu, X (eds. 2019. Cytotoxicity assays: Methods to measure dead cells. In Assay guidance manual. Eli Lilly & Company and the National Center for Advancing Translational Sciences, Bethesda (MD).
62. Shortt E, Lourido S. 2020. Plate-based quantification of stimulated *Toxoplasma egress*. Methods Mol Biol 2071:171–186. https://doi.org/10.1007/978-1-4939-9857-9_10
63. Sugi T, Kobayashi K, Takemae H, Gong H, Ishiwa A, Murakoshi F, Recuenco FC, Iwanaga T, Horimoto T, Akashi H, Kato K. 2013. Identification of mutations in TgMAPK1 of *Toxoplasma gondii* conferring resistance to 1NM-PP1. Int J Parasitol Drugs Drug Resist 3:93–101. https://doi.org/10.1016/j.ijpddr.2013.04.001
64. Long S, Brown KM, Drewry LL, Anthony B, Phan IQH, Sibley LD. 2017. Calmodulin-like proteins localized to the conoid regulate motility and cell invasion by *Toxoplasma gondii*. PLoS Pathog 13:e1006379. https://doi.org/10.1371/journal.ppat.1006379
65. Brown KM, Long S, Sibley LD, Weiss LM. 2017. Plasma membrane association by N-acylation governs PKG function in*Toxoplasma gondii* . mBio 8. https://doi.org/10.1128/mBio.00375-17
66. Nishimura K, Fukagawa T, Takisawa H, Kakimoto T, Kanemaki M. 2009. An auxin-based degron system for the rapid depletion of proteins in nonplant cells. Nat Methods 6:917–922. https://doi.org/10.1038/nmeth.1401
67. Lourido S, Zhang C, Lopez MS, Tang K, Barks J, Wang Q, Wildman SA, Shokat KM, Sibley LD. 2013. Optimizing small molecule inhibitors of calcium-dependent protein kinase 1 to prevent infection by *Toxoplasma gondii*. J Med Chem 56:3068–3077. https://doi.org/10.1021/jm4001314
68. Drewry LL, Sibley LD. 2019. The Hitchhiker's guide to parasite dissemination. Cell Microbiol 21:e13070–15. https://doi.org/10.1111/cmi.13070
69. Leung JM, Rould MA, Konradt C, Hunter CA, Ward GE. 2014. Disruption of TgPHIL1 alters specific parameters of *Toxoplasma gondii* motility measured in a quantitative, three-dimensional live motility assay. PLoS One 9:e85763. https://doi.org/10.1371/journal.pone.0085763

70. Gaji RY, Johnson DE, Treeck M, Wang M, Hudmon A, Arrizabalaga G. 2015. Phosphorylation of a myosin motor by TgCDPK3 facilitates rapid initiation of motility during *Toxoplasma gondii* egress. PLoS Pathog 11:e1005268. https://doi.org/10.1371/journal.ppat.1005268
71. Lovett JL, Marchesini N, Moreno SNJ, Sibley LD. 2002. *Toxoplasma gondii* microneme secretion involves intracellular Ca(2+) release from inositol 1,4,5-triphosphate (IP(3))/ryanodine-sensitive stores. J Biol Chem 277:25870–25876. https://doi.org/10.1074/jbc.M202553200
72. Govindasamy K, Bhanot P. 2020. Overlapping and distinct roles of CDPK family members in the pre-erythrocytic stages of the rodent malaria parasite, *Plasmodium berghei*. PLoS Pathog 16:e1008131. https://doi.org/10.1371/journal.ppat.1008131
73. Bansal Abhisheka, Ojo KK, Mu J, Maly DJ, Van Voorhis WC, Miller LH, Boothroyd JC, Doerig C, Duraisingh M. 2016. Reduced activity of mutant calcium-dependent protein kinase 1 is compensated in *Plasmodium falciparum* through the action of protein kinase G. mBio 7. https://doi.org/10.1128/mBio.02011-16
74. Bansal A, Molina-Cruz A, Brzostowski J, Liu P, Luo Y, Gunalan K, Li Y, Ribeiro JMC, Miller LH. 2018. PfCDPK1 is critical for malaria parasite gametogenesis and mosquito infection. Proc Natl Acad Sci USA 115:774–779. https://doi.org/10.1073/pnas.1715443115
75. Winterbach W, Van Mieghem P, Reinders M, Wang H, de Ridder D. 2013. Topology of molecular interaction networks. BMC Syst Biol 7:90. https://doi.org/10.1186/1752-0509-7-90
76. Huynh M-H, Carruthers VB, Boothroyd JC. 2006. *Toxoplasma* MIC2 is a major determinant of invasion and virulence. PLoS Pathog 2:e84. https://doi.org/10.1371/journal.ppat.0020084
77. Boucher LE, Bosch J. 2015. The apicomplexan glideosome and adhesins - structures and function. J Struct Biol 190:93–114. https://doi.org/10.1016/j.jsb.2015.02.008
78. Broncel M, Dominicus C, Vigetti L, Nofal SD, Bartlett EJ, Touquet B, Hunt A, Wallbank BA, Federico S, Matthews S, Young JC, Tate EW, Tardieux I, Treeck M. 2020. Profiling of myristoylation in *Toxoplasma gondii* reveals an N-myristoylated protein important for host cell penetration. Elife 9:e57861. https://doi.org/10.7554/eLife.57861
79. Foe IT, Child MA, Majmudar JD, Krishnamurthy S, van der Linden WA, Ward GE, Martin BR, Bogyo M. 2015. Global analysis of palmitoylated proteins in *Toxoplasma gondii*. Cell Host & Microbe 18:501–511. https://doi.org/10.1016/j.chom.2015.09.006
80. Amos B, Aurrecoechea C, Barba M, Barreto A, Basenko EY, Bażant W, Belnap R, Blevins AS, Böhme U, Brestelli J, Brunk BP, Caddick M, Callan D, Campbell L, Christensen MB, Christophides GK, Crouch K, Davis K, DeBarry J, Doherty R, Duan Y, Dunn M, Falke D, Fisher S, Flicek P, Fox B, Gajria B, Giraldo-Calderón GI, Harb OS, Harper E, Hertz-Fowler C, Hickman MJ, Howington C, Hu S, Humphrey J, Iodice J, Jones A, Judkins J, Kelly SA, Kissinger JC, Kwon DK, Lamoureux K, Lawson D, Li W, Lies K, Lodha D, Long J, MacCallum RM, Maslen G, McDowell MA, Nabrzyski J, Roos DS, Rund SSC, Schulman SW, Shanmugasundram A, Sitnik V, Spruill D, Starns D, Stoeckert CJ, Tomko SS, Wang H, Warrenfeltz S, Wieck R, Wilkinson PA, Xu L, Zheng J. 2022. Veupathdb: the eukaryotic pathogen, vector and host bioinformatics resource center. Nucleic Acids Res 50:D898–D911. https://doi.org/10.1093/nar/gkab929
81. Ishino T, Orito Y, Chinzei Y, Yuda M. 2006. A calcium-dependent protein kinase regulates plasmodium ookinete access to the midgut epithelial cell. Mol Microbiol 59:1175–1184. https://doi.org/10.1111/j.1365-2958.2005.05014.x
82. Gurnett AM, Liberator PA, Dulski PM, Salowe SP, Donald RGK, Anderson JW, Wiltsie J, Diaz CA, Harris G, Chang B, Darkin-Rattray SJ, Nare B, Crumley T, Blum PS, Misura AS, Tamas T, Sardana MK, Yuan J, Biftu T, Schmatz DM. 2002. Purification and molecular characterization of cGMP-dependent protein kinase from apicomplexan parasites. A novel chemotherapeutic target. J Biol Chem 277:15913–15922. https://doi.org/10.1074/jbc.M108393200
83. Huynh M-H, Carruthers VB. 2009. Tagging of endogenous genes in a *Toxoplasma gondii* strain lacking Ku80. Eukaryot Cell 8:530–539. https://doi.org/10.1128/EC.00358-08
84. Smith TA, Lopez-Perez GS, Herneisen AL, Shortt E, Lourido S. 2022. Screening the *Toxoplasma kinome* with high-throughput tagging identifies a regulator of invasion and egress. Nat Microbiol 7:868–881. https://doi.org/10.1038/s41564-022-01104-0
85. Bastin P, Bagherzadeh Z, Matthews KR, Gull K. 1996. A novel EPITOPE tag system to study protein targeting and organelle biogenesis in *Trypanosoma brucei*. Mol Biochem Parasitol 77:235–239. https://doi.org/10.1016/0166-6851(96)02598-4
86. Dobrowolski JM, Carruthers VB, Sibley LD. 1997. Participation of myosin in gliding motility and host cell invasion by *Toxoplasma gondii*. Mol Microbiol 26:163–173. https://doi.org/10.1046/j.1365-2958.1997.5671913.x
87. Waldman BS, Schwarz D, Wadsworth MH II, Saeij JP, Shalek AK, Lourido S. 2020. Identification of a master regulator of differentiation in Toxoplasma. Cell 180:359–372. https://doi.org/10.1016/j.cell.2019.12.013
88. Starnes GL, Jewett TJ, Carruthers VB, Sibley LD. 2006. Two separate, conserved acidic amino acid domains within the *Toxoplasma gondii* Mic2 cytoplasmic tail are required for parasite survival. J Biol Chem 281:30745–30754. https://doi.org/10.1074/jbc.M606523200
89. Burg JL, Perelman D, Kasper LH, Ware PL, Boothroyd JC. 1988. Molecular analysis of the gene encoding the major surface antigen of *Toxoplasma gondii*. J Immunol 141:3584–3591.
90. Plattner F, Yarovinsky F, Romero S, Didry D, Carlier MF, Sher A, Soldati-Favre D. 2008. *Toxoplasma profilin* is essential for host cell invasion and Tlr11-dependent induction of an Interleukin-12 response. Cell Host Microbe 3:77–87. https://doi.org/10.1016/j.chom.2008.01.001